Article

Optimization strategy of novel peptide-based Michael acceptors for the treatment of Human African Trypanosomiasis

Roberta Ettari, Santo Previti, Santina Maiorana, Giorgio Amendola, Annika Wagner, Sandro Cosconati, Tanja Schirmeister, Ute A. Hellmich, and Maria Zappalà

J. Med. Chem., **Just Accepted Manuscript** • DOI: 10.1021/acs.jmedchem.9b00908 • Publication Date (Web): 12 Nov 2019

Optimization strategy of novel peptide-based Michael acceptors for the treatment of Human African Trypanosomiasis

*Roberta Ettari, *† Santo Previti,† Santina Maiorana,† Giorgio Amendola,‡ Annika Wagner,▽□ Sandro Cosconati,‡ Tanja Schirmeister,⊥ Ute A. Hellmich▽□ and Maria Zappalà†

†Department of Chemical, Biological, Pharmaceutical and Environmental Sciences, University of Messina, Italy, Viale Annunziata, 98168 Messina, Italy

‡DiSTABiF, University of Campania Luigi Vanvitelli, Via Vivaldi 43, 81100 Caserta, Italy

▽Centre for Biomolecular Magnetic Resonance (BMRZ), Max von Laue Str. 9, Frankfurt, DE 60438 Germany

□ Institute of Pharmacy and Biochemistry, University of Mainz, Johann-Joachim-Becherweg 30, Mainz, DE 55128 Germany

⊥Institute of Pharmacy and Biochemistry, University of Mainz, Staudingerweg 5 Mainz, DE 55128 Germany

ABSTRACT

This paper describes an optimization strategy of the highly active vinyl ketone **3** which was recognized as a strong inhibitor of rhodesain of *T. b. rhodesiense*, endowed with a k_{2nd} value of 67000·x 10^3 M^{-1} min^{-1} coupled with a high binding affinity (K_i = 38 pM). We now report a new structure-activity relationship study based on structural variations on the P3, P2 and P1' sites which led us to identify two potent lead compounds, i.e vinyl ketones **4h** and **4k**. Vinyl ketone **4h** showed an impressive potency towards rhodesain (k_{2nd}=881100 x 10^3) coupled to a good antiparasitic activity (EC_{50} =3.6 μM), while vinyl ketone **4k** proved to possess the highest binding affinity towards the trypanosomal protease (K_i=0.6 pM) and a submicromolar antiparasitic activity (EC_{50}= 0.67 μM), thus representing new lead compounds in the drug discovery process for the treatment of Human African Trypanosomiasis.

INTRODUCTION

Human African Trypanosomiasis (HAT), well-known as sleeping sickness, is a protozoan disease endemic in more than 30 countries in sub-Saharan Africa, where it continues to be an significant cause of illness and death, mainly in the rural areas, despite the substantial decrease of new cases reported in the last years.[1]

The etiological agents of HAT are two *Trypanosoma* subspecies: *T. brucei gambiense* is predominant in central and western Africa, where it causes a chronic form of HAT, whereas *T. brucei rhodesiense* is widespread in southern and eastern Africa, where it is responsible of an acute form of Trypanosomiasis, characterized by a fast onset and a high mortality.[2]

In this disease, which is transmitted by the bite of tsetse flies of the *Glossina* genus, two different stages could be recognized. The first one is known as hemolymphatic stage: the protozoan is initially present in the bloodstream (BS) and subsequently invades the hemolymphatic system, and thus causes

fever, myalgia and weakness. The hemolymphatic stage normally persists for weeks or months and, if untreated, can evolve into the second stage, during which the protozoan penetrates the blood-brain barrier (BBB), inducing neurological disturbances, sleep/wake cycle alterations, coma and finally death.[3]

To date, an effective vaccine has not yet been developed; this can be partially ascribed to the fast turnover of the variant surface glycoproteins (VSGs) present on the coat of the parasite that induces a high level of antigenic variations.[4] Consequently, the sole possible approach to treat this pathology is represented by the chemotherapy. At present, five drugs are available for HAT treatment: suramin and pentamidine, active in the hemolymphatic stage since they are unable to pass through the blood-brain barrier due to unfavorable physicochemical properties; as well as melarsoprol, eflornithine and nifurtimox, which are active in the neurological stage. Nevertheless, melarsoprol induces a reactive encephalopathy in 5-10% cases treated whereas eflornithine is active only against *T. b. gambiense*.[5] Currently, a combination of eflornithine and nifurtimox, represents the first-choice therapy of the neurological-stage of the disease caused by *T. b. gambiense.* Moreover, on 15 November 2018, a positive opinion has been adopted by the Committee for Medicinal Products for Human Use on the approval of fexinidazole to treat the *gambiense trypanosomiasis*.[6-8]

In this scenario, there is a pressing demand of identifying new targets and new effective drugs for HAT treatment.

In this context, rhodesain, a Clan CA, family C1 (papain-family) cathepsin L-like cysteine protease of *T. brucei rhodesiense*, represents one of the most promising targets for the development of new anti-HAT drugs.[9-11] The importance of rhodesain is rooted in its diverse functions: it is required to cross the BBB, thus inducing the neurological stage of HAT,[12] it is involved in the turnover of the trypanosome VSGs,[13] which form a densely packed coat surrounding the parasite and whose periodic antigenic variation allows the parasite to evade the host immune system. In addition, one of rhodesain extracellular activities is the degradation of host anti-VSG immunoglobulins, which further contributes to reduce the host immune response.[14-15] Lastly, rhodesain also takes part in the lysosomal

proteolysis of both protozoan proteins and host proteins transported inside the parasite.[16] All these functions clearly highlight the relevance of rhodesain both for *Trypanosoma* survival and at the same time for the progression of the disease.

The structure of rhodesain resembles that of other proteases of the papain family, with the catalytic triad, C25/H162/N182, situated in a cleft between two domains, named left (L) and right (R). Two crystal structures of rhodesain in complex with K11777 (**1**) and K11002 (**2**) (Chart 1), two potent irreversible rhodesain inhibitors with a peptidyl vinyl sulfone structure, have been deposited in the Protein Data Bank (PDB) (codes 2P7U[17] and 2P86[18]). These structural studies were fundamental to understand the key requisites for the binding of the inhibitors to the trypanosomal cysteine protease.

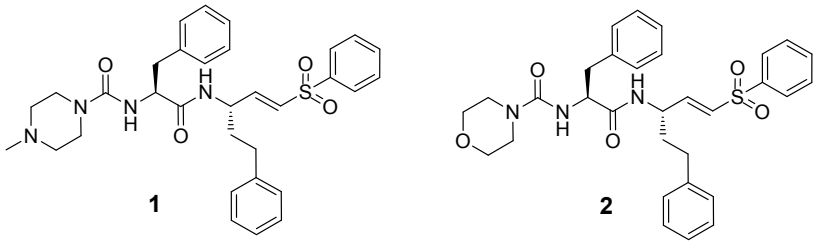

Chart 1. Structure of vinyl sulfones **1** and **2**.

In the last decade, our group has been involved in research projects aimed at identifying new inhibitors of rhodesain.[19-26] In particular, starting from the structure of vinyl sulfones **1-2**, we recently synthesized a number of dipeptidyl derivatives with different electrophilic portions as Michael acceptors, and identified as lead compound the vinyl ketone **3** (see chart 2),[26] a potent rhodesain covalent inhibitor which showed a k_{2nd} value of 67000·x 10^3 M^{-1} min^{-1} coupled with a high binding affinity (K_i = 38 pM). On the basis of the structure of the lead compound **3**, a new series of Michael acceptors has been designed (Chart 2). Here, we retained the vinyl ketone warhead and the homophenylalanine (hPhe) at the P1 site, whereas at the P3 site we introduced an *N*-methylpiperazine or a morpholine moiety in agreement to the structures of **1** and **2** (i.e. compounds **4a-b**). We then decided to replace the Cbz group with some benzo-fused rings (i.e. **4c-e**), one of which is the 2,3-dihydrobenzo[*b*][1,4]dioxine moiety (i.e. **4c**) present in potent rhodesain inhibitors reported in literature.[27] A panel of aromatic moieties, variously decorated with halogen atoms (i.e. **4f-m**), were

also introduced at the P3 site, in agreement to the structure of peptidic inhibitors bearing at the P3 site 3,5-difluoro- or 4-CF_3-phenyl moieties[28] or taking into consideration non peptide rhodesain inhibitors based on a triazine nucleus variously decorated with halogen–substituted aromatic nuclei.[29] This approach could also allow us to investigate the size of S3 pocket and to concurrently allow for the formation of halogen bonds and/or hydrophobic interactions. We also evaluated the relevance of the Phe residue at the P2 site, by synthesizing the hPhe analog (i.e. **4n**). A final study was also performed on the P1' site, thus synthesizing the corresponding ethyl analog of the lead compound **3** (i.e. **4o**), so as to explore the size of S1' pocket.

In this paper, we describe the approach to synthesize the inhibitors **4a-o,** together with the results of the biological investigation against rhodesain and *T. b. brucei* as well as molecular modeling studies.

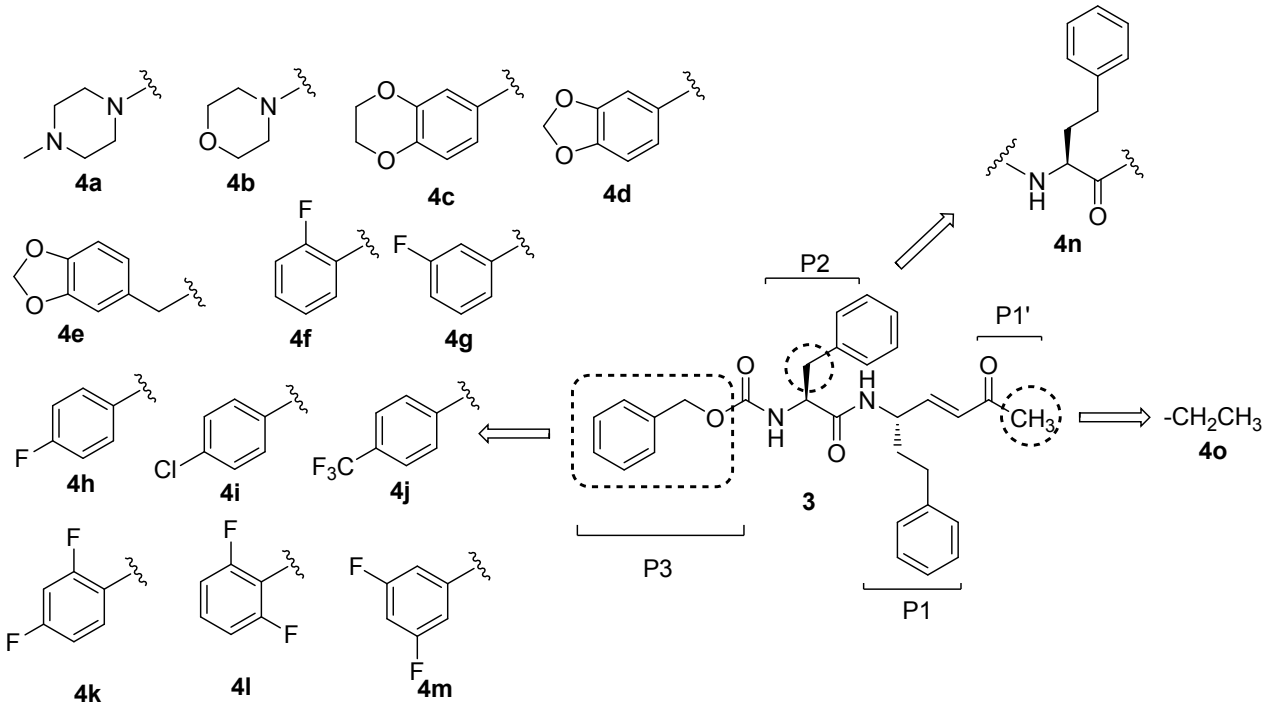

Chart 2. SAR study carried out starting on the lead compound **3**.

RESULTS AND DISCUSSION

Chemistry. The synthesis of compounds **4a-m** (Scheme 1) was carried out starting from methyl esters **5a-m**. Hydrolysis with LiOH provided the carboxylic acids **6a-m**. Amine **7**, obtained as

previously reported,[30] was reacted with carboxylic acids **6a-m** using HOBt and EDCI as coupling reagents, to provide the terminal olefins **8a-m**. Cross-metathesis (CM) reaction between **8a-m** and methyl vinyl ketone **9**, in the presence of 2nd generation Hoveyda-Grubbs catalyst and under microwave irradiation,[31] yielded the desired Michael acceptors **4a-m**.

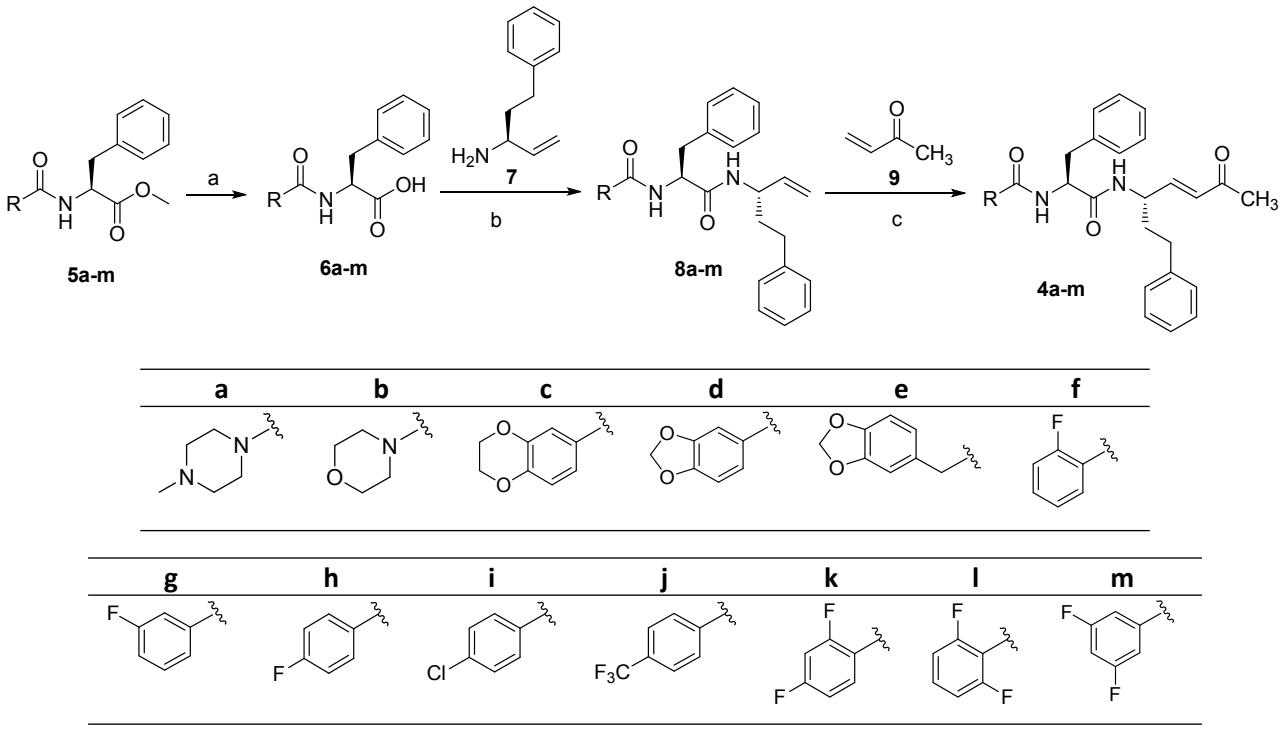

Scheme 1. Reagents and conditions: a) LiOH, MeOH/H_2O/dioxane (1:1:1), 0° C, 10 min, then rt, 12h; b) HOBt, EDCI, dry DMF/CH_2Cl_2 (1:1), 0°C, 10 min, then DIPEA, **7**, rt, 12h; e) 2nd generation Hoveyda-Grubbs catalyst, dry CH_2Cl_2, 100 °C, MW, 2-4h.

Compound **4n** was synthesized (Scheme 2) following the same procedure described above starting from carboxylic acid **10**. Similarly, compound **4o** (Scheme 3) was obtained from the terminal olefin **12**,[26] using the commercially available ethyl vinyl ketone **13**, as CM partner.

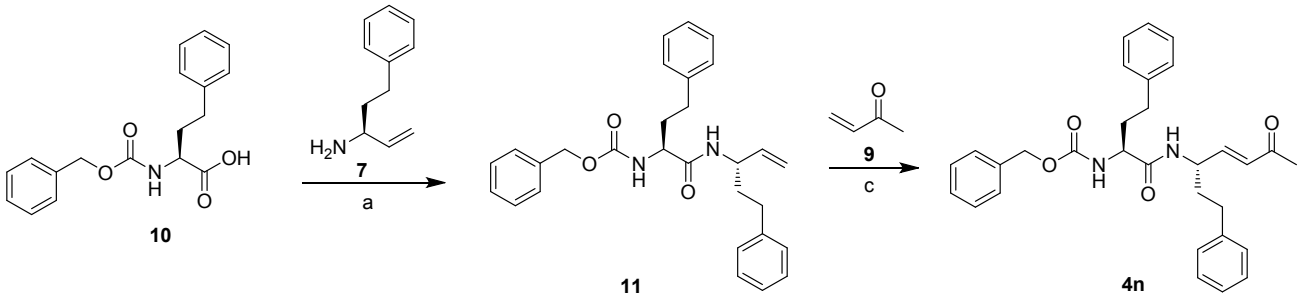

Scheme 2. Reagents and conditions: a) HOBt, EDCI, dry DMF/CH_2Cl_2 (1:1), 0°C, N_2, then 10 min DIPEA, **7**, rt, 12h; b) 2nd generation Hoveyda-Grubbs catalyst, dry CH_2Cl_2, 100 °C, MW, 2 h.

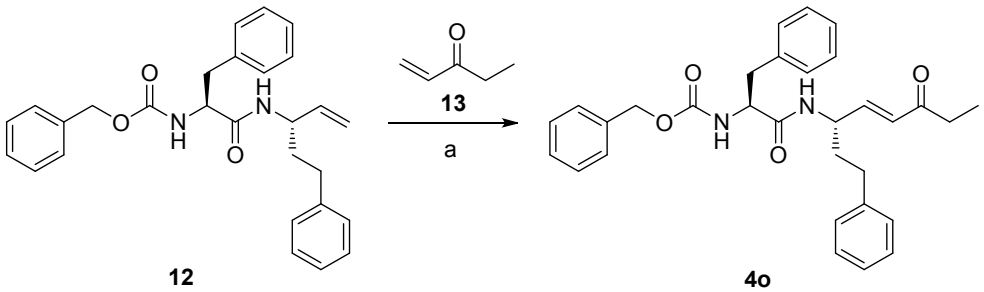

Scheme 3. Reagents and conditions: a) 2nd generation Hoveyda-Grubbs catalyst, dry CH_2Cl_2, 100 °C, MW, 2h.

Biological activity. The activity of all the synthesized compounds **4a-o** against recombinant rhodesain has been assessed by means of a fluorimetric assay, employing Cbz-Phe-Arg-AMC as fluorogenic substrate.[32] DMSO has been used as negative control whereas E-64 (**14**),[33] a well-known irreversible inhibitor of cysteine proteases of the papain family, has been employed as positive control. The preliminary screening, realized at a fixed inhibitor concentration (*i.e.* 50 μM), showed that all the tested compounds inhibited the target enzyme by 85%-100%.

We then performed continuous assays, by testing the compounds at seven diverse concentrations ranging from the one that minimally inhibits to that which totally inhibits the enzyme; the hyperbolic progress curves obtained (see e.g. **4h**, Figure 1) are indicative of an irreversible inhibition, in agreement with literature data of related compounds containing the same warheads.[32] Therefore, the following kinetic parameters have been measured: i) the dissociation constant (K_i) of the enzyme-inhibitor non-covalent complex [E·I] as a measure of the binding affinity; ii) the first-order rate constant of inhibition (k_{inac} min^{-1}) or inactivation rate constant as a measure of the rate of formation of the covalent adduct E-I; iii) the second-order rate constant of inhibition (k_{2nd} $M^{-1}min^{-1}$), obtained from the ratio k_{inac}/K_i, which is generally considered to be the best measure of relative inhibitor potency or effectiveness,[34] together with the K_i value which is the measure of the affinity towards the enzyme.

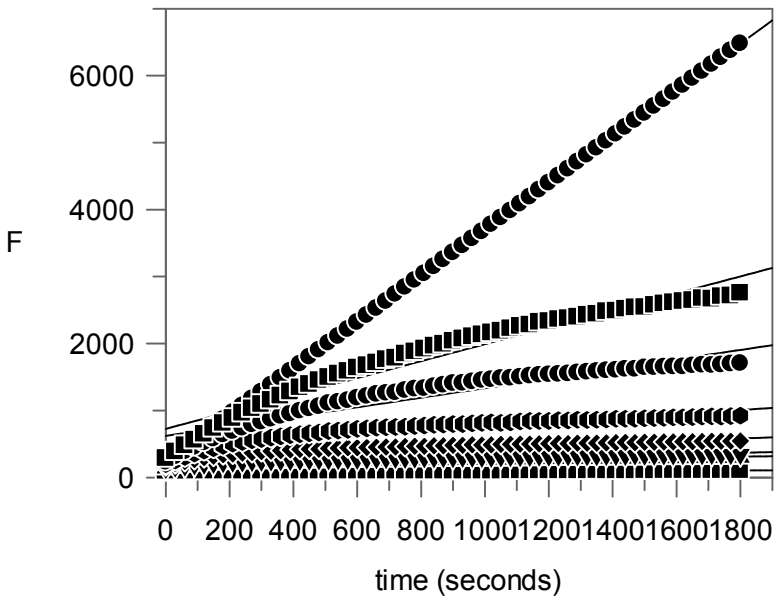

Figure 1. Progress curves of substrate hydrolysis in the presence of the inhibitor **4h**. Inhibitor concentrations (from top to bottom): 0, 0.005, 0.010, 0.025, 0.050, 0.075, 0.1, 0.5 nM.

A survey of the data reported in Table 1 shows that the introduction of the *N*-methyl piperazine (i.e. **4a**) or morpholine (i.e. **4b**) nuclei resulted in a strong reduction of potency (between 2-3 order of magnitude), with respect to the lead compound **3**. A slight reduction in activity was observed also in the case of compounds **4c** and **4d**, which bear a 2,3-dihydrobenzo[*b*][1,4]dioxine and a benzo[*d*][1,3]dioxole group at the P3 site, respectively. It is worth noting that when the benzo-fused nucleus at the P3 site is directly linked to the amide portion, the inhibitory properties are enhanced. In contrast, compound **4e**, with a methylene spacer between the amide moiety and the benzo[*d*][1,3]dioxole nucleus, showed a k_{2nd} value between one and two orders of magnitude lower with respect to compound **4d** (i.e. k_{2nd}15300 x $10^3 M^{-1}$ $min^{-1}$and 435 x $10^3 M^{-1}$ $min^{-1}$for **4d** and **4e**, respectively).

A survey of the results of rhodesain inhibition of compounds **4f-m** put in evidence that the substitution pattern on the phenyl at the P3 position has a remarkable impact on the inhibition of the target protease. If we consider the K_i values, which express the affinity of the inhibitor for the enzyme, the 2,4-difluoro substituted derivative **4k**, with its subpicomolar binding affinity (K_i = 0.6 pM) gave the best results.

If we consider the k_{2nd} value, which is the measure of the potency of the inhibitor, the 4-fluoroderivative **4h** turned out to be the most potent derivative of the series with an impressive k_{2nd} value of 881100 x 10^3 M^{-1} min^{-1}, with respect to those of the other monosubstituted derivatives **4f-g** and **4i-j**. All in all, we can conclude that the optimal substitution pattern on the phenyl is represented by the presence of electron withdrawing fluorine atom or CF_3 group located at 2 or 4 position.

Interestingly, the structural modifications realized on the lead compound **3** allowed to improve its potency, as shown by the vinyl ketones **4f-4h and 4j-4m**. It is worth noting that the most active compounds **4h** and **4k** showed improved k_{2nd} values towards rhodesain with respect to that of the lead compound **3**, coupled with a consistent improvement also of the binding affinity (i.e. K_i values 1.1 pM (**4h**) and 0.6 pM (**4k**) *vs* 38 pM of compound **3**).

Concerning the P2 site, the replacement of the Phe residue with a hPhe (i.e. **4n**) seemed to be unfruitful for the enhancement of the inhibitory properties. The same trend was observed when the methyl group of the vinyl ketone warhead, present at the P1' site, was replaced with an ethyl group (i.e. **4o**).

To check the selectivity towards the target enzyme, all the synthesized compounds were tested against cathepsin L, the closest human homolog to rhodesain. A survey of the results of this assay (Table 2) evidenced that all the tested compounds are weaker inhibitors of cathepsin L than they are of rhodesain. The best results have been obtained with derivatives **4g, 4k** and **4l** that showed k_{2nd} values against cathepsin L three or four orders of magnitude inferior than those reported for the inhibition of the trypanosomal protease. It is worth noting that compound **4k** which showed the best affinity to rhodesain (i.e. K_i=0.0006 nM) showed also the best selectivity profile.

For compounds with the highest k_{2nd} values, an in vitro assay against *T. b. brucei* cultures has been performed (Table 3). Compounds **4d**, **4h**, **4i** and **4m** were used in concentrations from 16.7 μM to 32.5 nM in consecutive dilutions in two independent triplicates at two timepoints (24 and 48 h). EC_{50} values of all four compounds are in a low micromolar range from 3.2 ± 0.5 μM to 5.1 ± 1.0 μM.

At the same time we tested also compound **4k**, which showed the highest binding affinity (K_i=0.6 pM) towards rhodesain, obtaining a submicromolar EC_{50} value (0.67 μM) against the parasite. Interestingly, when we tested also compound **4n**, which showed a lower binding affinity (K_i=5.5 nM), we also obtained a submicromolar activity against the parasite. This good antiparasitic activity could be justified by a increased cell permeability of the inhibitor or with the possibility to target another crucial cysteine protease of *T. b. rhodesiense*, i.e. TbCatB.

However, the lack of a proper match between the enzyme inhibition properties and the antitrypanosomal activity is a problem that often occurs in medicinal chemistry field, reported in literature also in the case of the most promising rhodesain inhibitors.[10] In the case of peptidyl inhibitors, one problem could be the susceptibility to the enzymatic hydrolysis: in this context, a higher stability can be achieved, for example, by modifying the stereochemistry of the aminoacids (i.e. from L to D-aminoacids) or by inserting non-natural amino acids (e.g. β-aminoacids, N-methyl-aminoacids) into the peptide scaffold. Another issue could be a low cellular uptake: in this case, both the incorporation of an inhibitor into nanoparticles or prodrug approaches, e.g. to gain affinity toward membrane transporters, could enhance the intracellular uptake. All these opportunities will be considered in the near future with the ultimate goal of turning a potent rhodesain inhibitor into a potent antitrypanosomal drug.

Table 1. Activity of compounds 4a-4o towards rhodesain

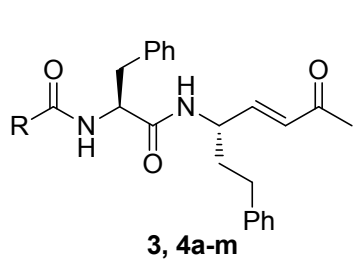

3, 4a-m

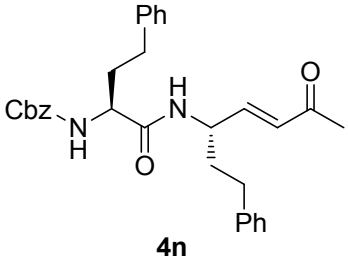

4n

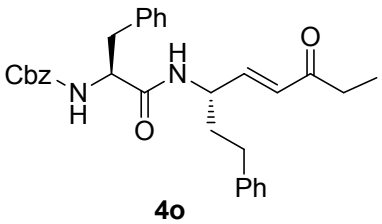

4o

Comp	R	Rhodesain		
		k_{inac} (min^{-1})	K_i(nM)	k_{2nd} (x 10^3 M^{-1} min^{-1})
4a	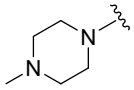	0.00042±0.00012	1.8±0.9	266±70
4b	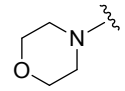	0.00049±0.00011	3.1±0.6	157±7
4c	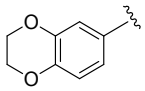	0.0043±0.0032	0.74±0.62	7200±1800
4d	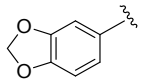	0.0005±0.0001	0.034±0.011	15300±2200
4e	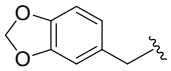	0.00085±0.00025	2.10±0.98	435±83
4f	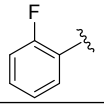	0.0006±0.0001	0.003±0.001	230300±86200
4g	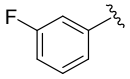	0.0032±0.0005	0.023±0.008	149200±27900
4h	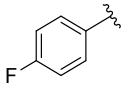	0.0009±0.00002	0.0011±0.0002	881100±102450
4i	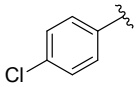	0.0008±0.0001	0.029±0.002	29300±6300
4j	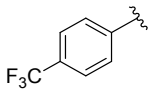	0.00075±0.00005	0.0044±0.0005	174700±31400
4k	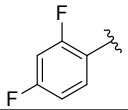	0.00007±0.00003	0.0006±0.0003	107100±2200
4l	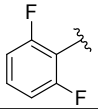	0.0012±0.0001	0.0076±0.001	150800±6500
4m	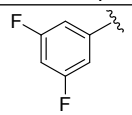	0.0016±0.0006	0.015±0.008	112600±18600
4n	-	0.00072±0.00017	5.5±1.9	137±16

4o	-	0.00082±0.000025	0.50±0.15	1800±481
3[26]	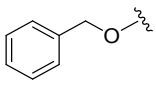	0.00255 ± 0.00075	0.038 ± 0.011	67000 ± 432
14[26]		0.009 ± 0.0004	35 ± 5	261 ± 27
1[10]	-	-	-	9000

Table 2. Activity of compounds 4a-o towards Cathepsin L.

Comp	Cathepsin L		
	k_{inac} (min^{-1})	K_i (nM)	k_{2nd} (x 10^3 M^{-1} min^{-1})
4a	0.0047±0.0005	158.3±42.5	31±5
4b	0.0039±0.0001	174.8±29.8	23±3
4c	0.0076±0.0010	78.2±20.9	102±14
4d	0.0016±0.0001	10.2±0.2	157±3
4e	0.0053±0.0002	90.3±6.8	59±2
4f	0.0011±0.0000	5.3±3.2	313±183
4g	0.0019±0.0000	47±7	41±6
4h	0.0018±0.0001	1.5±0.2	1228±136
4i	0.0018±0.0001	0.60±0.06	3030 ±303
4j	0.0015±0.0001	4.1±0.3	380±37
4k	0.0015±0.0001	35±14	52±19
4l	0.002±0.0002	230±65	8.9±1.6
4m	0.0022±0.0001	14.8±3.3	156±34
4n	0.0056 ±0.0002	453.0±43.9	12.0±0.8
4o	0.0071±0.0007	108.2±21.5	67±6

Table 3. Antitrypanosomal activity of selected rhodesain inhibitors

Comp	*T. brucei brucei* EC_{50} (μM)	
	24 h	48 h
4d	5.0 ± 0.9	3.7 ± 0.4
4h	5.1 ± 1.0	3.6 ± 0.2
4i	4.8 ± 0.5	3.2 ± 0.5
4k	0.74 ± 0.21	0.67 ± 0.26
4m	4.0 ± 0.8	3.4 ± 0.9
4n	0.55 ± 0.12	0.44 ± 0.15
3[26]	3.2 ± 2.2	3.0 ± 1.2

Molecular Modeling.

To elucidate the structural basis of inhibition of the novel compounds, docking studies were performed. For these *in silico* experiments, the same AutoDock4.2 (AD4) covalent docking protocol successfully employed in our previous work was used (See Materials and Methods).[26,35-37] Thus, the compounds **4a-o** were all covalently docked into the crystal structure of rhodesain (PDB code 2P86)[18] through residue C25. The binding pose of the inhibitor featuring best k_{2nd} **4h** in the active site of rhodesain is shown in Figure 2.

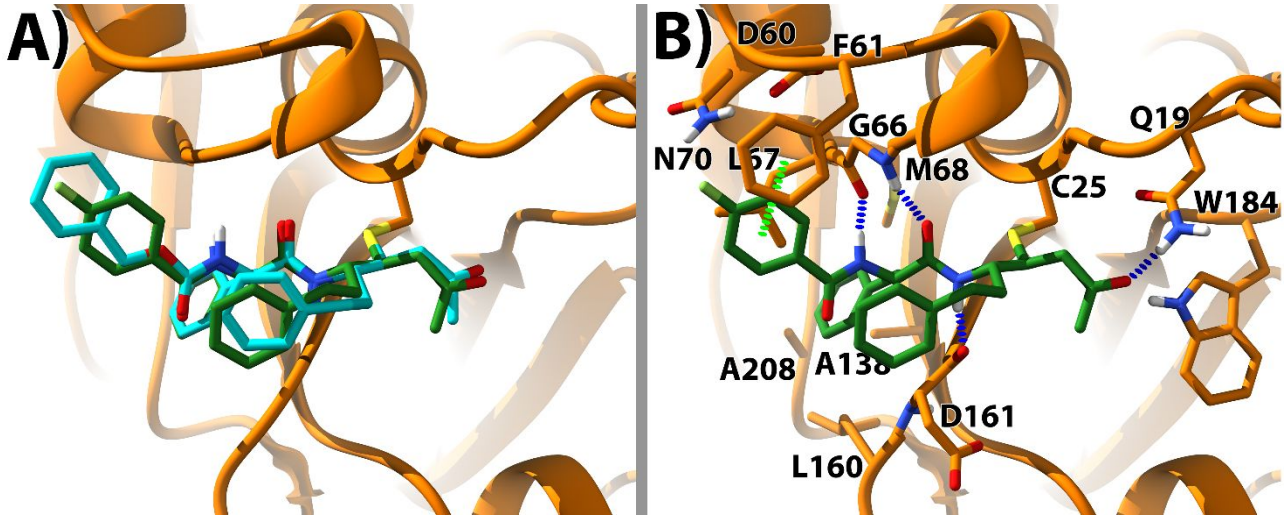

Figure 2. a) Superimposition of compounds **3**[26] (cyan sticks) and **4h** (green sticks) docked conformations in rhodesain (orange ribbons). b) Rhodesain/**4h** theoretical complex. The enzyme is depicted as orange ribbons and sticks, while the ligand as green sticks. Important residues are labelled. H-bonds are shown in blue dashed lines. The π-stacking interaction is shown in light green dashed lines. Information on the distances of all calculated non-bonded ligand/enzyme interactions are reported in SI (Table S1).

The achieved docked conformations for all the studied compounds are in accordance with our previous study.[26] In particular, the ligands establish a tight network of H-bonds within the active site. The backbone atoms of G66 engage in a double bridged H-bond interaction with the ligand P2 CO and NH atoms. The backbone NH of P1 is involved in a H-bond with the backbone CO of D161. Furthermore, the ketone warhead accepts a H-bond from Q19 sidechain, while W184 sidechain might form a second H-bond with the ketone warhead. Of note, the longer alkyl chain featured by compound **4o** is partially solvent exposed and would point towards the hydrophilic side chain of D161, possibly

accounting for its lower activity. Instead, the Phe P2 moiety is favorably lodged in the hydrophobic S2 gorge lined by M68, A138, L160, and A208 residues. Analogously, AD4 calculates for **4n** a binding pose that generally resembles the one obtained for **4h**, with the exception of the long hPhe P2 residue, which is more solvent exposed and less prone to fill the S2 cavity of the enzyme, thereby explaining the lower inhibitory activity of **4n**.

As for the P3 moieties, they generally fit in the S3 cleft lined by residues D60, F61, L67, and N70. According to our docking study, the sole exception to this trend is represented by compound **4e**, whose bulky P3 portion was found to be lodged in the S2 region of the active site, with the Phe P2 placed in the S3 cleft. Possibly, this switch between S2 and S3 of the P2 and P3 residues could be energetically disfavored, causing a decrease in affinity. Interestingly, in the case of the P3 aromatic substituents of **4c-d** and **4f-m**, a parallel-displaced π-stacking interaction can be observed with F61. Such an interaction should be enhanced in compounds **4f-m**, featuring substituents with electron-withdrawing groups. It is also worth noting that in compounds **4c-d** and **4f-m** the aromatic ring is directly connected to an amide portion. This latter portion engages in a H-bond with G66, as we mentioned before. Therefore, it could be postulated that, given the overall electronic conjugation, electron-withdrawing groups at position 4 of the aromatic substituent (**4h**, **4j**, and **4k**), would enhance the strength of the H-bond to G66.[38] Additionally, the 4-fluorine atoms in **4h**, **4j**, and **4k** are also located in a possible H-bonding position with N70. Nevertheless, while compound **4j** features an electron-withdrawing 4-CF_3, it can also be argued that its high electron density would cause in this position an unfavorable contact with the nearby acidic D60, this should explain why **4j** is a less potent enzyme inhibitor. Moreover, in compound **4g,** 3-F atom should be less efficacious in enhancing the H-bond to G66. Thus, the 4-fluorine atom in P3 (**4h** and **4k**) seems to be the most productive substitution to yield high inhibitory potency at rhodesain.

The drug-likeness of compounds for which the antitrypanosomal was assessed (compounds **3**, **4d**, **4h**, **4i, 4k**, **4m**, and **4n)** was *in silico* evaluated through the QikProp tool, part of the Schrödinger suite (Schrödinger Release 2019-1: QikProp, Schrödinger, LLC, New York, NY, 2019). The latter is useful

to predict several physicochemical and pharmacokinetic parameters of a given compound, and the results are also compared to the values obtained for the 95% of marketed drugs. The summary of the calculated values are reported in Table 3.

Table 3. Calculated Physicochemical and Pharmacokinetic Properties of Compounds 3, 4d, 4h-k, 4m-n.

Parameter	3	4d	4h	4i	4k	4m	4n	Range of recommended values[a]
#rotor[b]	12	11	11	11	11	11	13	0 – 15
#rtvFG[c]	1	2	1	1	1	1	1	0 – 2
Lipinski Rule of 5 violations[d]	1	1	1	1	1	1	1	N.A.
mol_MW[e]	484.6	498.6	472.6	489.0	490.6	490.5	498.6	130.0 – 725.0
dipole[f]	6.7	3.6	2.4	2.3	5.2	3.1	10.7	1.0 – 12.5
SASA[g]	893.1	806.9	833.8	849.0	835.8	837.2	917.6	300.0–1000.0
donorHB[h]	1.3	1.3	1.3	1.3	1.3	1.3	1.3	0.0 – 6.0
accptHB[i]	6.3	7.8	6.3	6.3	6.3	6.3	6.3	2.0 – 20.0
QPlogPo/w[j]	6.1	4.9	5.8	6.0	5.8	5.9	6.6	-2.0 – 6.5
QPlogS[k]	-7.3	-5.5	-6.7	-7.1	-6.9	-6.9	-8.3	–6.5 – 0.5
QPPCaco[l]	522.7	795.0	739.0	738.8	568.2	578.1	1080.0	<25 poor, >500 great
QPlogBB[m]	-1.5	-1.1	-1.1	-1.0	-1.1	-1.1	-1.4	-3.0 – 1.2
QPPMDCK[n]	413.3	585.5	1053.2	1438.4	1182.5	1482.4	598.7	<25 poor, >500 great
Jorgensen Rule of 3 violations[o]	1	1	1	1	1	1	1	N.A.
#metab[p]	5	4	4	4	4	4	5	1 – 8
Human Oral Absorption[q]	100	100	100	100	100	100	100	<25% poor, >80% high

[a]For 95% of known drugs. [b]Number of non-trivial (not CX3), non-hindered (not alkene, amide, small ring) rotatable bonds. [c]Number of reactive functional groups. [d]Predicted numbers of violations of Lipinski's rule of five. [e]Molecular weight of the molecule. [f]Computed dipole moment of the molecule. [g]Total solvent accessible surface area (SASA) in square angstroms using a probe with a 1.4 Å radius. [h]Estimated number of hydrogen bonds that would be donated by the solute to water molecules in an aqueous solution. [i]Estimated number of hydrogen bonds that would be accepted by the solute from water molecules in an aqueous solution. [j]Predicted octanol/water partition coefficient. [k]Predicted aqueous solubility, log S. S in mol dm^{-3} is the concentration of the solute in a saturated solution that is in equilibrium with the crystalline solid. [l]Predicted apparent Caco-2 cell permeability in nm/sec. Caco-2 cells are a model for the gut-blood barrier. [m]Predicted brain/blood partition coefficient for orally delivered drugs. [n]Predicted apparent MDCK cell permeability in nm/sec. MDCK cells are considered to be a good mimic for the blood-brain barrier. [o]Predicted numbers of violations of Jorgensen rule of three. [p]Number of likely metabolic reactions. [q]Predicted qualitative human oral absorption percentage.

Indeed, all the compounds showed good drug-like properties with predicted 100% oral absorption, one violation of the Lipinski rule, one violation of the Jorgensen rule, and good lipophilic features. A general improvement with respect to the lead compound **3** was recorded for the predicted apparent MDCK and permeability in Caco-2 cell, and for the predicted coefficient of brain/blood partition, especially for compounds **4d**, **4h**, **4i**, **4k**, and **4m**. These data represent key features for an effective antitrypanosomal agent. Moreover, a prospective increase in the solubility is also reported for all the new compounds with the exception of **4n**. Indeed, the lipophilicity calculated for this latter compound might be conducive of a higher membrane penetration thereby explaining why, although being a less potent rhodesain inhibitor, this ligand has a submicromolar antitrypanosomal activity in cell-based experiments. Thus, compound **4h** and **4k** should meet all the necessary requirements to be good lead compounds for design and discovery of new antitrypanosomal agents.

CONCLUSIONS

In conclusion, we developed a new series of peptidyl vinyl ketones that were demonstrated to be inactivators of rhodesain at nanomolar/picomolar level, with an EC_{50} against cultured *T. b. brucei* in a low micromolar range. The vinyl ketone **4h**, with an impressive potency towards rhodesain (k_{2nd}=881100 x 10^3) coupled to a good antiparasitic activity (EC_{50} =3.6 μM), and the vinyl ketone **4k**, which showed the highest binding affinity (K_i=0.6 pM) and a submicromolar antiparasitic activity (EC_{50}= 0.67 μM), could certainly represent new lead compounds for the discovery of new drugs to treat Human African Trypanosomiasis.

EXPERIMENTAL SECTION

Chemistry. All reagents and solvents were obtained from commercial suppliers and were used without further purification. Reactions under microwave irradiation were performed on

a CEM Discover apparatus. Elemental analyses were carried out on a C. Erba Model 1106 (Elemental Analyzer for C, H and N) instrument, and the obtained results are within ± 0.4% of the theoretical values. Merck silica gel 60 F254 plates were used for analytical TLC; flash column chromatography was performed on Merck silica gel (200–400 mesh). ^{1}H-NMR spectra were recorded on a Varian 300 MHz NMR spectrometer. ^{13}C-NMR were obtained on a Varian 300 and 500 MHz NMR spectrometer, operating at frequencies of 75 or 125 MHz . The residual signal of the deuterated solvent was used as internal standard. Splitting patterns are described as singlet (s), doublet (d), doublet of doublet (dd), triplet (t), quartet (q), multiplet (m), or broad singlet (bs). ^{1}H and ^{13}C NMR chemical shifts (δ) are expressed in ppm and coupling constants (J) are given in Hz. Compounds **5a-m**,[32,39-43] **6a-d** and **6f-j**,[32,41,43-46] and **10**[47] were synthesized according to standard procedures and spectroscopic data are in agreement to those reported in literature.

4-Methyl-N-((S)-1-oxo-1-(((S,E)-6-oxo-1-phenylhept-4-en-3-yl)amino)-3-phenylpropan-2-yl)piperazine-1-carboxamide (4a). A solution of terminal olefin **8a** (1 equiv.) in dry CH_2Cl_2 (3 mL), in a 10 mL microwave tube equipped with a magnetic stirrer, was treated with methyl vinyl ketone **9** (10 equiv.) and 2nd generation Hoveyda–Grubbs catalyst [(1,3-bis-(2,4,6-trimethylphenyl)-2-imidazolidinylidene)-dichloro-(*o*-isopropoxyphenylmethylene) ruthenium] (0.1 equiv.) under microwave irradiation at 100°C for 4h. Subsequently, the solvent was removed under reduced pressure and the residue was purified by flash column chromatography using CH_2Cl_2/MeOH (9:1) as eluent mixture, to obtain Michael acceptor **4a**. Yield: 81%; R_f = 0.34 (CH_2Cl_2/MeOH, 9:1).

Consistency: white solid. ^{1}H NMR (300 MHz, $CDCl_3$) = δ: 1.82-1.99 (m, 2H), 2.23 (s, 3H), 2.29 (s, 3H), 2.32-2.43 (m, 4H), 2.54 (t, J = 7.7 Hz, 2H), 3.03-3.14 (m, 2H), 3.32-3.40 (m, 4H), 4.37-4.49 (m, 1H), 4.78-4.92 (m, 1H), 5.29 (d, J = 6.3 Hz, 1H), 5.86 (d, J = 7.6 Hz, 1H), 6.28 (d, J = 15.2 Hz, 1H), 6.91 (dd, J = 15.2 Hz, 5.2, 1H), 7.16-7.42 (m, 10H). ^{13}C NMR (125 MHz, $CDCl_3$) = δ: 28.89, 31.92, 36.37, 38.64, 43.52, 45.85, 51.29, 54.33, 56.09, 125.93, 126.93, 128.35, 128.40, 128.70, 129.40, 130.14, 137.18, 137.53, 148.19, 165.17, 172.32, 197.64. Elemental analysis calcd for $C_{28}H_{36}N_4O_3$: C 70.56; H 7.61; N 11.76. Found: C 70.41, H 7.33, N 12.02.

N-((S)-1-Oxo-1-((S,E)-6-oxo-1-phenylhept-4-en-3-ylamino)-3-phenylpropan-2-yl)morpholine-4-carboxamide (4b). Synthesis of Michael acceptor **4b** was carried out following the procedure described for compound **4a**, starting from terminal olefin **8b**. Yield: 84%; R_f = 0.27 (EtOAc/light petroleum, 3:2). Consistency: white solid. ^{1}H NMR (300 MHz, $CDCl_3$) = δ: 1.62-1.75 (m, 2H), 2.28 (s, 3H), 2.51 (t, J = 7.6 Hz, 2H), 2.98-3.11 (m, 2H), 3.21-3.34 (m, 4H), 3.49-3.64 (m, 4H), 4.34-4.47 (m, 1H), 4.72-4.83 (m, 1H), 5.37 (d, J = 6.6 Hz, 1H), 5.88 (d, J = 7.5 Hz, 1H), 6.31 (d, J = 15.2 Hz, 1H), 6.88 (dd, J = 15.2 Hz, 5.4, 1H), 7.11-7.38 (m, 10H). ^{13}C NMR (125 MHz, $CDCl_3$) = δ: 27.62, 32.11, 36.64, 39.14, 44.20, 51.55, 56.17, 66.50, 126.14, 127.05, 128.46, 128.51, 128.72, 129.64, 129.97, 137.82, 141.48, 145.38, 157.38, 171.59, 197.77. Elemental analysis calcd for $C_{27}H_{33}N_3O_4$: C 69.95; H 7.18; N 9.06. Found: C 70.24, H 7.42, N 8.87.

N-((S)-1-Oxo-1-(((S,E)-6-oxo-1-phenylhept-4-en-3-yl)amino)-3-phenylpropan-2-yl)-2,3-dihydrobenzo[b][1,4]dioxine-6-carboxamide (4c). Synthesis of Michael acceptor **4c** was carried out following the procedure described for compound **4a**, starting from terminal olefin **8c**, under microwave irradiation for 2 h. Yield: 87%; R_f = 0.17 (light petroleum/EtOAc, 1:1). Consistency: white solid. ^{1}H NMR (300 MHz, $CDCl_3$) = δ: 1.69-1.98 (m, 2H), 2.27 (s, 3H), 2.50 (t, J = 7.6 Hz, 2H), 2.96-3.17 (m, 2H), 4.22-4.46 (m, 5H), 4.59-4.71 (m, 1H), 5.39 (d, J = 6.4 Hz, 1H), 5.88 (d, J = 7.3 Hz, 1H),6.04 (d, J = 15.2 Hz, 1H), 6.67 (dd, J = 15.2, 6.0 Hz, 1H),7.06 (d, J = 1.6 Hz, 1H), 7.11-7.39 (m, 11H), 7.63 (d, J = 1.6 Hz, 1H). ^{13}C (75 MHz, $CDCl_3$) = δ: 26.83, 31.93, 36.41, 38.67, 51.94,

56.17, 64.20, 64.56, 116.52, 116.84, 120.89, 126.34, 126.74, 127.76, 128.07, 128.27, 128.69, 128.93, 130.77, 136.81, 141.35, 146.62, 147.86, 149.16, 166.90, 170.43, 197.65. Elemental analysis calcd for $C_{31}H_{32}N_2O_5$: C 72.64; H 6.29; N 5.47. Found: C 72.47, H 5.96, N 5.71.

N-((S)-1-Oxo-1-(((S,E)-6-oxo-1-phenylhept-4-en-3-yl)amino)-3-phenylpropan-2-yl)benzo[d][1,3]dioxole-5-carboxamide (4d). Synthesis of Michael acceptor **4d** was carried out following the procedure described for compound **4c**, starting from terminal olefin **8d**. Yield: 86%; R_f =0.70(light petroleum/EtOAc, 2:3). Consistency: white powder. ^{1}H NMR (300 MHz, $CDCl_3$) = δ: 1.62-1.89 (m, 2H), 2.20 (s, 3H), 2.56 (t, J = 7.6 Hz, 2H), 3.07-3.32 (m, 2H), 4.49-4.65 (m, 1H), 4.74-4.89 (m, 1H), 5.93 (d, J = 15.8 Hz, 1H), 6.02 (s, 2H), 6.23 (d, J = 7.6 Hz, 1H), 6.46 (dd, J = 15.8, 5.6 Hz, 1H), 6.69 (d, J = 6.4 Hz, 1H), 7.05 (d, J = 7.5 Hz, 2H), 7.13-7.38 (m, 11H). ^{13}C (125 MHz, $CDCl_3$) = 27.70, 31.81, 35.74, 38.04, 50.03, 55.19, 101.81, 107.59, 108.10, 121.86, 127.27, 127.60, 128.30, 128.52, 128.87, 129.25, 129.28, 129.30, 129.94, 136.46, 140.51, 145.27, 148.09, 166.77, 170.45, 197.87. Elemental analysis calcd for $C_{30}H_{30}N_2O_5$: C 72.27; H 6.06; N 5.62. Found: C 72.38; H 6.29; N 5.40.

(S)-2-(2-(Benzo[d][1,3]dioxol-5-yl)acetamido)-N-((S,E)-6-oxo-1-phenylhept-4-en-3-yl)-3-phenylpropanamide (4e). Synthesis of Michael acceptor **4e** was carried out following the procedure described for compound **4c**, starting from terminal olefin **8e**. Yield: 81%; R_f = 0.18 (light petroleum/EtOAc, 1:1). Consistency: white solid. ^{1}H NMR (300 MHz, $CDCl_3$) = δ: 1.66-1.92 (m, 2H), 2.24 (s, 3H), 2.54 (t, J = 7.8 Hz, 2H), 2.96-3.11 (m, 2H), 3.39 (s, 2H), 4.17-4.28 (m, 1H), 4.59-4.67 (m, 1H), 5.55 (d, J = 6.6 Hz, 1H), 5.89 (d, J = 7.3 Hz, 1H), 5.96 (s, 2H), 6.14 (d, J = 15.1 Hz, 1H), 6.69 (dd, J = 15.1, 6.1 Hz, 1H), 6.58-6.74 (m, 3H), 7.07-7.32 (m, 10H). ^{13}C NMR (75 MHz, $CDCl_3$) = δ: 27.51, 32.04, 38.21, 43.16, 51.54, 54.43, 101.17, 108.42, 109.49, 122.74, 125.80, 126.19, 128.29, 128.43, 128.62, 128.84, 129.66, 130.81, 136.42, 141.53, 146.95, 148.17, 149.24, 170.29, 171.33, 197.57. Elemental analysis calcd for $C_{31}H_{32}N_2O_5$: C 72.64; H 6.29; N 5.47. Found: C 72.40, H 6.55, 5.19.

2-Fluoro-N-((S)-1-oxo-1-(((S,E)-6-oxo-1-phenylhept-4-en-3-yl)amino)-3-phenylpropan-2-yl)benzamide (4f). Synthesis of Michael acceptor **4f** was carried out following the procedure described for compound **4c**, starting from terminal olefin **8f**. Yield*:* 60 %; Consistency: white powder*;* R_f = 0.15 (cyclohexane /EtOAc, 7:3); ^{1}H NMR (500 MHz, $CDCl_3$) = δ: 1.73-1.92 (m, 2H), 2.21 (s, 3H), 2.51-2.60 (m, 2H), 3.16 (dd, *J* = 13.7, 8.0 Hz, 1H), 3.23 (dd, *J* = 13.8, 6.5 Hz, 1H), 4.55-4.62 (m, 1H), 4.80-4.86 (m, 1H), 5.96 (dd, *J* = 16.0, 1.4 Hz, 1H), 6.07 (d, *J* = 8.3 Hz, 1H), 6.49 (dd, *J* = 16.0, 5.6 Hz, 1H), 7.05 (d, *J* = 7.1 Hz, 2H), 7.09-7.18 (m, 2H), 7.17-7.36 (m, 9H), 7.44-7.54 (m, 1H), 8.03 (td, *J* = 7.8, 1.7 Hz, 1H) ppm. ^{13}C NMR (125.73 MHz, $CDCl_3$) = δ: 27.75. 31.85, 35.75, 37.80, 50.00, 55.47, 116.23 (d, *J* = 24.5 Hz), 120.23, 124.89 (d, *J* = 3.3 Hz), 126.19, 127.26, 128.28, 128.50, 128.86, 129.32, 129.90, 131.85 (d, *J* = 1.8 Hz), 133.89 (d, *J* = 9.4 Hz), 136.35, 140.61, 145.31, 160.72 (d, *J* = 248.7 Hz), 163.53, 170.10, 197.88. Elemental analysis: calcd for $C_{29}H_{29}FN_2O_3$: C 73.71; H 6.19; N 5.93; found: C 71.60, H 6.22, N 5.92.

3-Fluoro-N-((S)-1-oxo-1-(((S,E)-6-oxo-1-phenylhept-4-en-3-yl)amino)-3-phenylpropan-2-yl)benzamide (4g) Synthesis of Michael acceptor **4g** was carried out following the procedure described for compound **4c**, starting from terminal olefin **8g**. Yield*:* 64 %; Consistency: white powder*; R*f = 0.21 (cyclohexane /EtOAc, 7:3); ^{1}H NMR (500 MHz, $CDCl_3$) = δ: 1.72-1.82 (m, 2H), 2.20 (s, 3H), 2.48 (d, *J* = 7.8 Hz, 2H), 3.11 (dd, *J* = 13.5, 8.5 Hz, 1H), 3.21 (dd, *J* = 13.6, 6.2 Hz, 1H), 4.49-4.60 (m, 1H), 4.82-4.93 (m, 1H), 5.91 (d, *J* = 16.0 Hz, 1H), 6.35 (d, *J* = 8.3 Hz, 1H), 6.45 (dd, *J* = 16.0, 5.8 Hz, 1H), 7.05 (dd, *J* = 15.6, 7.3 Hz, 2H), 7.10-7.31 (m, 10H), 7.33-7.41 (m, 1H), 7.42-7.52 (m, 2H) ppm. ^{13}C NMR (125.73 MHz, $CDCl_3$) = δ: 27.65, 31.84, 35.71, 38.36, 50.08, 55.25, 114.53 (d, *J* = 22.5 Hz), 119.03 (d, *J* = 21.2 Hz), 122.52 (d, *J* = 2.7 Hz), 126.22, 127.31, 128.25, 128.52, 128.84, 129.29, 130.01, 130.36 (d, *J* = 7.7 Hz), 135.72 (d, *J* = 6.9 Hz), 136.23, 140.50, 145.16, 163.73, 166.08, 170.32, 197.77 ppm. Elemental analysis: calcd for $C_{29}H_{29}FN_2O_3$: C 73.71; H 6.19; N 5.93; found: C 71.59, H 6.29, N 5.95.

4-Fluoro-N-((S)-1-oxo-1-(((S,E)-6-oxo-1-phenylhept-4-en-3-yl)amino)-3-phenylpropan-2-yl)benzamide (4h). Synthesis of Michael acceptor **4h** was carried out following the procedure described for compound **4c**, starting from terminal olefin **8h**. Yield: 84%; R_f =0.77(light petroleum/EtOAc, 2:3). Consistency: white powder. ^{1}H NMR (300 MHz, $CDCl_3$) = δ: 1.62-1.91 (m, 2H), 2.19 (s, 3H), 2.52 (t, J = 7.6 Hz, 2H), 3.06-3.27 (m, 2H), 4.49-4.63 (m, 1H), 4.85-4.99 (m, 1H), 6.10 (d, J = 15.8 Hz, 1H), 6.46 (dd, J = 15.8 Hz, 5.9, 1H), 6.51-6.71 (m, 1H), 6.99-7.37 (m, 13H), 7.67-7.81 (m, 2H). ^{13}C (125 MHz, $CDCl_3$) = δ: 27.67, 31.84, 35.47, 38.34, 50.05, 55.21, 115.76 (d, J = 21.9) 126.23, 127.29, 128.25, 128.52, 128.83, 129.29, 129.45 (d, J = 9.1), 129.67, 129.99, 136.30, 140.52, 145.20, 165.00 (d, J = 252.4), 166.42, 170.40, 197.57. Elemental analysis calcd for $C_{29}H_{29}FN_2O_3$: C 73.71; H 6.19; N 5.93. Found: C 73.65; H 6.32; N 5.61.

4-Chloro-N-((S)-1-oxo-1-(((S,E)-6-oxo-1-phenylhept-4-en-3-yl)amino)-3-phenylpropan-2-yl)benzamide (4i). Synthesis of Michael acceptor **4i** was carried out following the procedure described for compound **4c**, starting from terminal olefin **8i.** Yield*:* 82%; R_f =0.79 (light petroleum/EtOAc, 2:3). Consistency: white powder. ^{1}H NMR (300 MHz, $CDCl_3$) = δ: 1.62-1.92 (m, 2H), 2.20 (s, 3H), 2.52 (t, J = 7.6 Hz, 2H), 3.06-3.26 (m, 2H), 4.49-4.61 (m, 1H), 4.84-4.98 (m, 1H), 6.10 (d, J = 15.8 Hz, 1H), 6.45 (dd, J = 15.8 Hz, 5.4, 1H), 6.53-6.66 (m, 1H), 6.99-7.12 (m, 2H), 7.13-7.42 (m, 11H), 7.60-7.75 (m, 2H). ^{13}C (125 MHz, $CDCl_3$) = δ: 27.68, 31.84, 35.72, 38.35, 50.07, 55.23, 126.24, 127.31, 128.25, 128.50, 128.53, 128.84, 128.94, 129.29, 130.01, 131.85, 136.23, 138.35, 140.49, 145.15, 166.37, 170.34, 197.77. Elemental analysis calcd for $C_{29}H_{29}ClN_2O_3$: C 71.23; H 5.98; N 5.73. Found: C 71.65; H 5.82; N 5.60.

N-((S)-1-Oxo-1-(((S,E)-6-oxo-1-phenylhept-4-en-3-yl)amino)-3-phenylpropan-2-yl)-4-trifluoromethylbenzamide (4j). Synthesis of Michael acceptor **4j** was carried out following the procedure described for compound **4c**, starting from terminal olefin **8j**. Yield: 78 %; Consistency: white powder*;* R_f = 0.22 (cyclohexane/EtOAc, 7:3); ^{1}H NMR (500 MHz, $CDCl_3$) = δ: 1.76-1.93 (m, 2H), 2.21 (s, 3H), 2.50 (d, J = 7.8 Hz, 2H), 3.11 (dd, J = 13.4, 8.4 Hz, 1H), 3.23 (dd, J = 13.5, 6.3 Hz,

1H), 4.51-4.62 (m, 1H), 4.79-4.90 (m, 1H), 5.92 (d, *J* = 16.0 Hz, 1H), 6.24 (d, *J* = 8.1 Hz, 1H), 6.45 (dd, *J* = 16.0, 5.8 Hz, 1H), 7.01-7.10 (m, 2H), 7.11-7.33 (m, 9H), 7.67 (d, *J* = 7.9 Hz, 2H), 7.83 (d, *J* = 7.7 Hz, 2H) ppm. ^{13}C NMR (125.73 MHz, $CDCl_3$) = δ: 27.70, 31.83, 35.70, 38.38, 50.14, 55.31, 123.57 (q, *J* = 272.7 Hz), 125.66 (q, *J* = 3.7 Hz), 126.27, 127.39, 127.55, 128.54, 128.89, 129.07, 128.89, 129.27, 130.06, 133.46 (q, *J* = 32.6 Hz), 136.13, 140.43, 145.24, 166.05, 170.14, 197.78. Elemental analysis: calcd for $C_{30}H_{29}F_3N_2O_3$: C 68.95; H 5.59; N 5.36; found: C 68.99, H 5.46, N 5.52.

2,4-Difluoro-N-((S)-1-oxo-1-(((S,E)-6-oxo-1-phenylhept-4-en-3-yl)amino)-3-phenylpropan-2-yl)benzamide (4k). Synthesis of Michael acceptor **4k** was carried out following the procedure described for compound **4c**, starting from terminal olefin **8k**. Yield*:*65 %; Consistency: white powder*;* R_f = 0.40 (cyclohexane /EtOAc, 6:4); ^{1}H NMR (300 MHz, $CDCl_3$) = δ: 1.71-1.92 (m, 2H), 2.21 (s, 3H), 2.50 (d, *J* = 7.8 Hz, 2H), 3.13 (dd, *J* = 13.5, 8.2 Hz, 1H), 3.22 (dd, *J* = 13.6, 6.2 Hz, 1H), 4.52-4.64 (m, 1H), 4.78-4.91 (m, 1H), 5.95 (d, *J* = 15.9 Hz, 1H), 6.09-6.17 (m, 1H), 6.42-6.52 (m, 1H), 6.82-6.93 (m, 1H), 6.94-7.01 (m, 1H), 7.02-7.11 (m, 2H), 7.12-7.35 (m, 8H), 8.03 (dd, *J* = 8.4, 6.5 Hz, 1H) ppm. ^{13}C NMR (125.73 MHz, $CDCl_3$) = δ: 27.71, 31.84, 35.74, 38.10, 50.03, 55.50, 112.38, 104.50 (dd, *J* = 28.2, 25.7 Hz), 112.48 (dd, *J* = 20.9, 3.1 Hz), 126.21, 127.29, 128.25, 128.51, 128.84, 129.30, 129.96, 136.23, 137.8, 140.57, 145.25, 162.53, 166.16, 166.93, 170.06, 197.80 ppm. Elemental analysis: calcd for $C_{29}H_{28}F_2N_2O_3$: C 71.01; H 5.75; N 5.71; found: C 71.21, H 5.54, N 5.50.

2,6-Difluoro-N-((S)-1-oxo-1-(((S,E)-6-oxo-1-phenylhept-4-en-3-yl)amino)-3-phenylpropan-2-yl)benzamide (4l). Synthesis of Michael acceptor **4l** was carried out following the procedure described for compound **4c**, starting from terminal olefin **8l**. Yield*:* 66%; Consistency: white powder*;* R_f = 0.39 (cyclohexane /EtOAc, 6:4); ^{1}H NMR (500 MHz, $CDCl_3$) = δ:1.73-1.90 (m, 2H), 2.18 (s, 3H), 2.52-2.64 (m, 2H), 3.15 (dd, *J* = 13.7, 8.0 Hz, 1H), 3.23 (dd, *J* = 13.7, 6.4 Hz, 1H), 4.53-4.63 (m, 1H), 4.93 (dd, *J* = 14.4, 7.8 Hz, 1H), 5.91 (dd, *J* = 16.0, 1.4 Hz, 1H), 6.27 (d, *J* = 8.4 Hz, 1H),

6.46 (dd, *J* = 16.0, 5.6 Hz, 1H), 6.68 (d, *J* = 7.8 Hz, 1H), 6.88-6.97 (m, 2H), 7.07 (d, *J* = 8.0 Hz, 2H), 7.13 (dd, *J* = 10.6, 4.1 Hz, 1H), 7.18-7.32 (m, 7H), 7.32-7.42 (m, 1H) ppm. ^{13}C NMR (125.73 MHz, $CDCl_3$) = δ: 27.73, 31.82, 35.61, 38.03, 49.99, 55.14, 112.09 (dd, *J* = 21.1, 4.4 Hz), 113.36 (d, *J* = 19.5 Hz), 126.11, 127.24, 128.33, 128.48, 128.77, 129.35, 129.79, 132.18 (t, *J* = 10.4 Hz), 136.06, 140.72, 145.24, 159.93 (dd, *J* = 253.1, 6.5 Hz), 160.42, 169.67, 197.84 ppm. Elemental analysis: calcd for $C_{29}H_{28}F_2N_2O_3$: C 71.01; H 5.75; N 5.71; found: C 71.25, H 5.56, N 5.52.

3,5-Difluoro-N-((S)-1-oxo-1-(((S,E)-6-oxo-1-phenylhept-4-en-3-yl)amino)-3-phenylpropan-2-yl)benzamide (4m). Synthesis of Michael acceptor **4m** was carried out following the procedure described for compound **4c**, starting from terminal olefin **8m**. Yield: 83%; R_f = 0.27 (light petroleum/EtOAc, 4:1). Consistency:white solid. ^{1}H NMR (300 MHz, $CDCl_3$) = *δ*: 1.86-1.97 (m, 2H), 2.23 (s, 3H), 2.55 (t, *J* = 7.8 Hz, 2H), 3.01-3.22 (m, 2H), 4.16-4.29 (m, 1H), 4.51-4.60 (m, 1H), 5.36 (bs, 1H), 5.94 (d, *J* = 8.3 Hz, 1H), 6.01 (d, *J* = 15.2 Hz, 1H), 6.54 (dd, *J* = 15.2, 6.1 Hz, 1H), 7.02-7.11, (m, 1H), 7.16-7.32 (m, 8H), 7.44-7.57 (m, 4H). ^{13}C (125 MHz, $CDCl_3$) = *δ*: 26.54, 32.14, 36.86, 38.41, 51.18, 56.67, 107.22 (t, *J* = 25.9 Hz), 110.59 (dd, *J* = 28.0, 3.7 Hz), 126.24, 126.97, 128.54, 128.79, 129.04, 129.51, 130.83, 136.78, 137.12, 141.29, 149.39, 163.51 (dd, *J* = 251.2, 9.8 Hz), 164.94, 170.22, 197.58. Elemental analysis calcd for $C_{29}H_{28}F_2N_2O_3$: C 71.01; H 5.75; N 5.71. Found: C 70.86, H 5.97, N 5.93.

*Benzyl ((S)-1-oxo-1-((S,E)-6-oxo-1-phenylhept-4-en-3-ylamino)-4-phenylbutan-2-yl)carbamate **(4n)**.* Synthesis of Michael acceptor **4n** was carried out following the procedure described for compound **4c**, starting from terminal olefin **11**. Yield:86%; R_f = 0.26 (light petroleum/EtOAc, 7:3). Consistency:white powder. ^{1}H NMR (300 MHz, $CDCl_3$) = *δ*: 1.71-2.01 (m, 4H), 2.21 (s, 3H), 2.53-2.72 (m, 4H), 4.02-4.20 (m, 1H), 4.53-4.70 (m, 1H), 5.10 (s, 2H), 5.26 (d, *J* = 7.4 Hz, 1H), 6.12 (d, *J* = 15.6 Hz, 1H), 6.30 (d, *J* = 6.9 Hz, 1H), 6.63 (dd, *J* = 15.6, 4.6 Hz, 1H), 7.02-7.42 (m, 15H). ^{13}C NMR (75 MHz, $CDCl_3$) = *δ*: 27.56, 31.71, 31.97, 32.48, 35.67, 49.91, 54.45, 67.23, 126.23, 126.25, 128.04, 128.31, 128.34, 128.44, 128.48, 128.56, 128.59, 129.88, 135.91, 140.40, 140.65, 145.74,

156.39, 171.02, 197.92; Elemental analysis calcd for $C_{31}H_{34}N_2O_4$: C 74.67; H 6.87; N 5.62. Found: C 74.91, H 7. 04, N 5.47.

Benzyl ((S)-1-oxo-1-(((S,E)-6-oxo-1-phenyloct-4-en-3-yl)amino)-3-phenylpropan-2-yl)carbamate (4o). Synthesis of Michael acceptor **4o** was carried out following the procedure described for compound **4c** starting from terminal olefin **12**,[22] which was treated with CM partner **13**, commercially available. Yield:86%; R_f = 0.28 (light petroleum/EtOAc, 7:3). Consistency: white solid. ^{1}H NMR (300 MHz, $CDCl_3$) = δ: 1.10 (t, J = 7.2 Hz, 3H), 1.67-1.96 (m, 2H), 2.33-2.64 (m, 4H), 2.99-3.15 (m, 2H), 4.32-4.48 (m, 1H), 4.50-4.67 (m, 1H), 5.10 (s, 2H), 5.38 (d, J = 5.4 Hz, 1H), 5.88-6.07 (m, 1H), 5.96 (d, J = 15.8 Hz, 1H), 6.52 (dd, J = 15.8, 5.5 Hz, 1H), 7.04-7.40 (m, 15H). ^{13}C NMR (75 MHz, $CDCl_3$) = δ: 27.94, 32.04, 34.85, 35.87, 38.11, 51.04, 56.63, 67.21, 126.33, 127.22, 128.04, 128.38, 128.41, 128.63, 128.67, 128.86, 129.32, 130.04, 135.95, 136.21, 141.01, 146.13, 156.14, 170.47, 199.73. Elemental analysis calcd for $C_{31}H_{34}N_2O_4$: C 74.67, H 6.87, N 5.62. Found C 74.89, H 6.63, N 5.86.

(S)-2-(2-(Benzo[d][1,3]dioxol-5-yl)acetamido)-3-phenylpropanoic acid (6e). To a solution of **5e** (1 equiv.) in a mixture of methanol/water/dioxane (1:1:1), LiOH as powder (3 equiv.) was added at 0°C. The reaction mixture was then stirred at rt for 12h. After this time, the solvents were evaporated in *vacuo*. The residue was treated with 10% solution citric acid (x 2), and the organic phase was extracted with EtOAc (x 3), dried over Na_2SO_4 and concentrated to afford the pure carboxylic acid **6e**. Yield: 94%; R_f = 0.04 (light petroleum/EtOAc, 1:1). Consistency: white solid. ^{1}H NMR (300 MHz, CD_3OD) = δ: 2.86 (dd, J = 13.8, 5.9 Hz, 1H), 3.17 (dd, J = 13.8, 5.9 Hz, 1H), 3.39 (s, 2H), 4.66 (dd, J = 13.8, 5.9 Hz, 1H), 5.91 (s, 2H), 6.58-6.74 (m, 3H), 7.08-7.24 (m, 5H).

(S)-2-(2,4-Difluorobenzamido)-3-phenylpropanoic acid (6k). Synthesis of acid **6k** was carried out following the procedure described for compound **6e** starting from ester **5k**. *Yield: 98 %;* Consistency*: white solid;* ^{1}H NMR (500 MHz, $CDCl_3$) = δ: 3.23 (dd, J = 14.0, 6.3 Hz, 1H), 3.34 (dd,

J = 14.0, 5.4 Hz, 1H), 5.06 – 5.11 (m, 1H), 6.87 – 6.79 (m, 1H), 6.97 (dt, *J* = 16.5, 4.8 Hz, 1H), 7.10 (dd, *J* = 12.2, 7.2 Hz, 1H), 7.18 – 7.34 (m, 5H), 8.04 – 8.11 (m, 1H).

(S)-2-(2,6-Difluorobenzamido)-3-phenylpropanoic acid (6l). Synthesis of acid **6l** was carried out following the procedure described for compound **6e** starting from ester **5l**. *Yield: 99 %;* Consistency: *white solid;* ^{1}H NMR (500 MHz, $CDCl_3$) = δ: 3.26 (dd, *J* = 14.1, 5.4 Hz, 1H), 3.38 (dd, *J* = 14.3, 5.7 Hz, 1H), 5.08 – 5.21 (m, 1H), 6.49 (bd, *J* = 6.7 Hz, 1H), 6.93 (t, *J* = 8.2 Hz, 2H), 7.19 – 7.42 (m, 6H).

(S)-2-(3,5-Difluorobenzamido)-3-phenylpropanoic acid (6m). Synthesis of acid **6m** was carried out following the procedure described for compound **6e** starting from ester **5m**. Yield: 96%; R_f = 0.02 (light petroleum/EtOAc, 9:1). Consistency: white solid. ^{1}H NMR (300 MHz, CD_3OD) = δ: 3.07 (dd, *J* = 13.9, 10.1 Hz, 1H), 3.35 (dd, *J* = 13.9, 4.9 Hz, 1H), 4.84 (dd, *J* = 10.1, 4.9 Hz, 1H), 7.06-7.37 (m, 8H).

4-Methyl-N-((S)-1-oxo-3-phenyl-1-((S)-5-phenylpent-1-en-3-ylamino)propan-2-yl)piperazine-1-carboxamide (8a). To a solution of carboxylic acid **6a** (1.2 equiv.) in DMF/CH_2Cl_2 (1:1) in nitrogen atmosphere, HOBt (1.2 equiv.) and EDCI (1.2 equiv.) were added at 0°C. After this time, DIPEA (1.5 equiv.) and amine **7**[30] (1 equiv.) were added and the reaction mixture was stirred over night at rt. Then, solvents were evaporated and the resulting residue was diluted with EtOAc, washed with brine (x 5), dried over Na_2SO_4, filtered and concentrated *in vacuo*. The crude product was purified by flash column chromatography using CH_2Cl_2/MeOH (9:1) as eluent mixture, to give the terminal olefin **8a**. Yield: 74%; R_f = 0.49 (CH_2Cl_2/MeOH, 9:1). Consistency: white solid. ^{1}H NMR (300 MHz, $CDCl_3$) = δ: 1.58-1.80 (m, 2H), 2.23 (s, 3H), 2.24-2.30 (m, 4H), 2.49 (t, *J* = 7.7 Hz, 2H),3.02-3.10 (m, 2H), 3.28-3.36 (m, 4H), 4.28-4.42 (m, 1H), 4.70 (q, *J* = 7.3 Hz, 1H). 4.87-5.08 (m, 2H), 5.51-5.65 (m, 2H), 6.99-7.29 (m, 11H).

N-((S)-1-Oxo-3-phenyl-1-(((S)-5-phenylpent-1-en-3-yl)amino)propan-2-yl)morpholine-4-carboxamide (8b). Synthesis of terminal olefin **8b** was carried out following the procedure described

for compound **8a**. Yield: 71%; R_f = 0.20 (light petroleum/EtOAc, 1:1). Consistency: white solid. ^{1}H NMR (300 MHz, $CDCl_3$) = δ: 1.58-1.71 (m, 2H), 2.46 (t, J = 7.8 Hz, 2H), 2.94-3.04 (m, 2H), 3.15-3.26 (m, 4H), 3.46-3.55 (m, 4H), 4.23-4.36 (m, 1H), 4.53 (q, J = 7.1 Hz, 1H), 4.80-4.99 (m, 2H), 5.31 (d, J = 6.2 Hz, 1H), 5.43-5.58 (m, 1H), 6.31 (d, J = 7.4 Hz, 1H), 6.97-7.26 (m, 10H).

N-((S)-1-Oxo-3-phenyl-1-((S)-5-phenylpent-1-en-3-ylamino)propan-2-yl)-2,3-dihydrobenzo[b][1,4]dioxine-6-carboxamide (8c). Synthesis of terminal olefin **8c** was carried out following the procedure described for compound **8a**, using **6c** as acid. Yield: 80%; R_f = 0.31 (light petroleum/EtOAc, 1:1). Consistency: white solid. ^{1}H NMR (300 MHz, $CDCl_3$) = δ: 1.68-1.94 (m, 2H), 2.52 (t, J = 7.6 Hz, 2H), 3.00-3.19 (m, 2H), 4.18-4.42 (m, 5H), 4.67-4.81 (m, 1H), 4.88-5.09 (m, 2H), 5.27 (d, J = 6.7 Hz, 1H), 5.58-5.70 (m, 1H), 5.88 (d, J = 7.3 Hz, 1H), 7.03 (d, J = 1.5 Hz, 1H), 7.12-7.22 (m, 7H), 7.25-7.34 (m, 4H), 7.63 (d, J = 1.5 Hz, 1H).

N-((S)-1-Oxo-3-phenyl-1-(((S)-5-phenylpent-1-en-3-yl)amino)propan-2-yl)benzo[d][1,3]dioxole-5-carboxamide (8d). Synthesis of terminal olefin **8d** was carried out following the procedure described for compound **8a**, using **6d** as acid. Yield: 70%; R_f= 0.49 (cyclohexane/EtOAc, 7:3). Consistency*:* white solid. ^{1}H NMR (300 MHz, $CDCl_3$) =δ: 1.55-1.83 (m, 2H), 2.48 (t, J = 8.2 Hz, 2H), 3.02-3.30 (m, 2H), 4.33-4.47 (m, 1H), 4.79-4.89 (m, 1H), 4.90-5.15 (m, 2H), 5.54-5.74 (m, 1H), 6.01 (s, 2H), 6.08-6.23 (m, 1H), 6.79 (d, J = 7.6 Hz, 1H), 6.88-7.02 (m, 1H), 7.04- 7.32 (m, 12 H).

(S)-2-(2-(Benzo[d][1,3]dioxol-5-yl)acetamido)-3-phenyl-N-((S)-5-phenylpent-1-en-3-yl)propanamide (8e). Synthesis of terminal olefin **8e** was carried out following the procedure described for compound **8a**, using **6e** as acid. Yield: 83%; R_f = 0.33 (light petroleum/EtOAc, 1:1). Consistency: white solid. ^{1}H NMR (300 MHz, $CDCl_3$) = δ: 1.59-1.81 (m, 2H), 2.51 (t, J = 7.6 Hz, 2H), 3.01-3.16 (m, 2H), 3.41 (s, 2H), 4.20-4.29 (m, 1H), 4.64-4.76 (m, 1H), 4.90-5.09 (m, 2H),5.44 (d, J = 6.8 Hz, 1H), 5.55-5.71 (m, 1H), 5.80 (d, J = 7.4 Hz, 1H),5.94 (s, 2H), 6.58-6.74 (m, 3H), 7.07-7.32 (m, 10H).

2-Fluoro-N-((S)-1-oxo-3-phenyl-1-(((S)-5-phenylpent-1-en-3-yl)amino)propan-2-yl)benzamide (8f). Synthesis of terminal olefin **8f** was carried out following the procedure described for compound **8a**, using **6f** as acid. Yield: 36%; Consistency*:* white crystals; R_f = 0.31 (light petroleum /EtOAc, 8:2); ^{1}H NMR (500 MHz, $CDCl_3$) = δ:1.67-1.83 (m, 2H), 2.54 (t, *J* = 7.8 Hz, 2H), 3.13 (dd, *J* = 13.7, 8.0 Hz, 1H), 3.25 (dd, *J* = 13.7, 6.2 Hz, 1H), 4.40 – 4.50 (m, 1H), 4.81 (ddd, *J* = 9.4, 8.0, 1.9 Hz, 1H), 4.93 – 5.08 (m, 2H), 5.61 (ddd, *J* = 17.1, 10.5, 5.8 Hz, 1H), 5.74 (d, *J* = 8.4 Hz, 1H), 7.06– 7.17 (m, 4H), 7.18 – 7.34 (m, 9H), 7.44-7.51 (m, 1H), 8.03 (td, *J* = 7.8, 1.9 Hz, 1H).

3-Fluoro-N-((S)-1-oxo-3-phenyl-1-(((S)-5-phenylpent-1-en-3-yl)amino)propan-2-yl)benzamide (8g). Synthesis of terminal olefin **8g** was carried out following the procedure described for compound **8a**, using **6g** as acid. Yield: 70%; Consistency*:* white crystals; *Rf* = 0.27 (light petroleum /EtOAc, 8:2); ^{1}H NMR (500 MHz, $CDCl_3$) = δ: 1.65-1.84 (m, 2H), 2.49 (t, *J* = 7.8 Hz, 2H), 3.09 (dd, *J* = 13.6, 8.7, 1H), 3.22 (dd, *J* = 13.7, 5.8 Hz, 1H), 4.34 – 4.48 (m, 1H), 4.73-4.85 (m, 1H), 4.94 (d, *J* = 17.2 Hz, 1H), 5.08 (m, 1H), 5.58 (ddd, *J* = 17.1, 10.5, 5.8 Hz, 1H), 5.72 (d, *J* = 8.3 Hz, 1H), 6.94 (d, *J* = 7.4 Hz, 1H), 7.02– 7.17 (m, 3H), 7.18 – 7.33 (m, 8H), 7.35-7.42 (m, 1H), 7.45-7.54 (m, 2H).

4-Fluoro-N-((S)-1-oxo-3-phenyl-1-(((S)-5-phenylpent-1-en-3-yl)amino)propan-2-yl)benzamide (8h). Synthesis of terminal olefin **8h** was carried out following the procedure described for compound **8a**, using **6h** as acid. Yield*:* 65%; *R*f = 0.62 (cyclohexane/EtOAc, 3:2). Consistency: white solid. ^{1}H NMR (300 MHz, $CDCl_3$) = δ: 1.57-1.89 (m, 3H), 2.49 (t, *J* = 7.9 Hz, 2H), 3.03-3.28 (m 2H), 4.34-4.48 (m, 1H), 4.84-5.22 (m, 3H), 5.52-5.78 (m, 1H), 6.97-7.35 (m, 13 H), 7.75 (dd, *J* = 8.6, 5.3 Hz, 2H).

4-Chloro-N-((S)-1-oxo-3-phenyl-1-(((S)-5-phenylpent-1-en-3-yl)amino)propan-2-yl)benzamide (8i). Synthesis of terminal olefin **8i** was carried out following the procedure described for compound **8a**, using **6i** as acid. Yield:68%; *R*f = 0.42 (light petroleum /EtOAc, 3:2). Consistency: white solid. ^{1}H NMR (300 MHz, $CDCl_3$) = δ: 1.64-1.86 (m, 3H), 2.50 (t, *J* = 7.9 Hz, 2H), 3.03-3.15 (m 1H), 3.17-3.29 (m, 1H), 4.33-4.48 (m, 1H), 4.71-4.87 (m, 1H), 4.89-5.16 (m, 1H), 5.51-5.88 (m,

2H), 6.93 (d, *J* = 7.0 Hz, 1H), 7.04-7.13 (m, 2H), 7.18-7.34 (m, 8H), 7.36-7.43 (m, 2H), 7.65-7.73 (m, 2H).

N-((S)-1-Oxo-3-phenyl-1-(((S)-5-phenylpent-1-en-3-yl)amino)propan-2-yl)-4-trifluoromethylbenzamide (8j). Synthesis of terminal olefin **8j** was carried out following the procedure described for compound **8a**, using **6j** as acid. Yield: 55%; Consistency*:* white solid; *Rf* = 0.55 (light petroleum /EtOAc, 8:2); ^{1}H NMR (500 MHz, $CDCl_3$) = δ: 1.66-1.85 (m, 2H), 2.50 (t, *J* = 8.1 Hz, 2H), 3.09 (dd, *J* = 13.8, 8.7 Hz, 1H), 3.24 (dd, *J* = 13.6, 5.8 Hz, 1H), 4.35–4.46 (m, 1H), 4.72-4.89 (m, 1H), 4.89-5.15 (m, 2H), 5.58 (ddd, *J* = 17.1, 10.5, 5.8 Hz, 1H), 5.64-5.86 (m, 2H), 7.04-7.34 (m, 11 H), 7.67 (d, *J* = 8.1 Hz, 2H), 7.85 (d, *J* = 8.1 Hz, 2H).

2,4-Difluoro-N-((S)-1-oxo-3-phenyl-1-((S)-5-phenylpent-1-en-3-ylamino)propan-2-yl)benzamide (8k). Synthesis of terminal olefin **8k** was carried out following the procedure described for compound **8a**, using **6k** as acid. Yield: 72%; Consistency*:* white powder; *Rf* = 0.28 (cyclohexane/EtOAc, 8:2); ^{1}H NMR (500 MHz, $CDCl_3$) = δ: 1.65-1.83 (m, 2H), 2.49 (t, *J* = 8.1 Hz, 2H), 3.11 (dd, *J* = 13.6, 8.2, 1H), 3.24 (dd, *J* = 13.7, 6.0 Hz, 1H), 4.43 (ddd, *J* = 13.7, 7.6, 6.2 Hz, 1H), 4.74-4.89 (m, 1H), 4.93-5.13 (m, 2H), 5.59 (ddd, *J* = 17.1, 10.4, 5.9 Hz, 1H), 5.72-5.90 (m, 1H), 6.84-6.90 (m, 1H), 6.94-6.99 (m, 1H), 7.05-7.17 (m, 3H), 7.18-7.33 (m, 8H), 8.00-8.09 (m, 1H).

2,6-Difluoro-N-((S)-1-oxo-3-phenyl-1-((S)-5-phenylpent-1-en-3-ylamino)propan-2-yl)benzamide (8l). Synthesis of terminal olefin **8l** was carried out following the procedure described for compound **8a**, using **6l** as acid. Yield: 78%; Consistency*:* white powder; *Rf* = 0.57 (cyclohexane/EtOAc, 7:3); ^{1}H NMR (500 MHz, $CDCl_3$) = δ: 1.68-1.88 (m, 2H), 2.49 (t, *J* = 7.8 Hz, 2H), 3.12 (dd, *J* = 13.7, 8.1, 1H), 3.18 (dd, *J* = 13.7, 8.1 Hz, 1H), 4.35-4.48 (m, 1H), 4.85 (dd, *J* = 14.0, 7.9 Hz, 1H), 4.89-5.13 (m, 2H), 5.59 (ddd, *J* = 17.1, 10.7, 6.0 Hz, 1H), 5.80 (d, *J* = 8.5 Hz, 1H), 6.66 (d, *J* = 7.6 Hz, 1H), 6.93 (t, *J* = 8.1 Hz, 2H), 7.06-7.42 (m, 11H).

3,5-Difluoro-N-((S)-1-oxo-3-phenyl-1-((S)-5-phenylpent-1-en-3-ylamino)propan-2-yl)benzamide (8m). Synthesis of terminal olefin **8m** was carried out following the procedure

described for compound **8a**, using **6m** as acid. Yield: 74%; R_f = 0.43 (light petroleum/EtOAc, 4:1). Consistency: white solid. ^{1}H NMR (300 MHz, $CDCl_3$) = δ: 1.88-1.98 (m, 2H); 2.58 (t, J = 7.6 Hz, 2H), 2.99-3.18 (m, 2H), 4.18-4.27 (m, 1H), 4.60-4.72 (m, 1H), 4.96-5.12 (m, 2H), 5.42 (d, J = 6.7 Hz, 1H), 5.57-5.70 (m, 1H), 5.86 (d, J = 8.3 Hz, 1H),6.98-7.09, (m, 1H), 7.18-7.34 (m, 8H), 7.40-7.51 (m, 4H).

Benzyl ((S)-1-oxo-4-phenyl-1-((S)-5-phenylpent-1-en-3-ylamino)butan-2-yl)carbamate (11). Synthesis of terminal olefin **11** was carried out following the procedure described for compound **8a**, using **10**[47] as acid. Yield: 79%; R_f = 0.41 (light petroleum/EtOAc, 9:1). Consistency: white powder. ^{1}H NMR (300 MHz, $CDCl_3$) = δ: 1.70-2.00 (m, 3H), 2.08-2.24 (m, 1H), 2.54-2.72 (m, 4H), 4.12 (dd, J = 14.3, 7.5 Hz, 1H), 4.42-4.56 (m, 1H), 5.03-5.22 (m, 2H), 5.09 (s, 2H), 5.32 (d, J = 7.6 Hz, 1H), 5.68-5.84 (m, 1H), 5.99 (d, J = 8.6 Hz, 1H), 7.09-7.37 (m, 15H).

Enzyme assays against rhodesain. Preliminary screening with rhodesain was performed with 50 µM inhibitor concentrations using an equivalent amount of DMSO as negative control. The enzyme was recombinantly expressed as previously described.[16,32,48-49] Product release from substrate hydrolysis (Cbz-Phe-Arg-AMC, 10 µM) was determined continuously over a period of 30 min. Compounds showing at least 85% inhibition at 50 µM were subjected to detailed assays. Second-order rate constants of inhibition were determined with 7 different inhibitor concentrations ranging from those that minimally inhibited to those that fully inhibited the enzyme. The assay buffer contains: 50 mM sodium acetate, pH = 5.5, 5 mM EDTA, 200 mM NaCl and 0.005 % Brij 35 to avoid aggregation and wrong-positive results. Enzyme buffer contains 5 mM DTT rather than Brij 35. Product formation was monitored continuously for 30 min at room temperature. To determine the first-order inactivation rate constants (k_{obs}) for the irreversible inhibition, progress curves (fluorescence (F) versus time) were analyzed by non-linear regression analysis using the equation F = A (1-exp (-k_{obs}t)) +B.[50] Fitting of the k_{obs} values against the inhibitor concentrations to the hyperbolic equation $k_{obs} = k_{inac}$ [I]/(K_{iapp}+[I]) gave the individual values of K_{iapp} and k_{inac}.[50] The K_{iapp}

values were corrected to zero substrate concentration by the term (1+[S]/K_m) in equation K_i = K_{iapp}/(1+[S]/K_m). The second-order rate constants k_{2nd} = k_{inac}/K_i were directly calculated from the individual constants. K_i and k_{inac} values were calculated by non-linear regression analyses using the program GraFit.[51] The K_m value used to correct K_{iapp} values was determined to 0.9 μM.[52] Inhibitor solutions were prepared from stocks in DMSO. Each independent assay was performed twice in duplicate in 96-well-plates in a total volume of 200 μL. Fluorescence of the product AMC of the substrate hydrolyses was measured using an Infinite 200 PRO microplate reader (Tecan, Männedorf, Switzerland) at room temperature with a 380 nm excitation filter and a 460 nm emission filter.

Enzyme assays against human cathepsin L. Assessment of activity against human cathepsin L of inhibitors was performed as previously described using the fluorogenic substrate Cbz-Phe-Arg-AMC.[30]

Cultivation and drug screening on *T. b. brucei* cultures. The BS parasites used in this work were of the *T. brucei brucei* 449 cell line, which is a descendant of the Lister 427 strain.[53] The cells were grown in HMI-9 medium supplemented with 10% (v/v) fetal calf serum, 50 units/mL penicillin/streptomycin and 0.2 μg/mL phleomycin at 37°C in a humidified atmosphere under 5% CO_2.[54] The antitrypanosomal activity was determined using the ATPlite assay[55] as described previously.[48] This assay is based on the adenosine triphosphate (ATP) dependent light emitting reaction catalyzed by firefly luciferase. In the presence of ATP and Mg ions, the enzyme transforms D-luciferine into D-luciferine adenylate which then turns into the excited keto form of oxyluciferin. ATP can be used as a marker for cell viability. All experiments were performed in white 96-well microplates (PerkinElmer). Each well was filled with 90 μL of medium containing 2500 cells/mL. Each tested compound (5 mM stock solutions) was then diluted in HMI-9 medium: firstly 1:3, then 1:10 and subsequently in ten 1:2 dilution steps using separate microplates. Of the final ten 1:2 dilutions, 10 μL each were then added to the 90 μL cell suspension, leading to an additional final 1:10 dilution for all compounds.[48] Addition of 10 μL DMSO corresponding to 10% DMSO, was used as a positive control. For drug addition, highest concentration of DMSO added was 0.3% DMSO. Addition of 0.3% DMSO served as a negative control. The plates

were incubated at 37 °C for 24 h and 48 h in two separate triplicates. 50 µL of ATPlite 1 step solution (PerkinElmer) was added to each well of the microplate, providing luciferin and luciferase as well as initiating cell lysis, and luminescence was measured in a Infinite® M200 PRO plate reader (Tecan Trading AG) at room temperature. A dose-response curve was obtained by plotting the measured values against the compound concentrations and the EC_{50} values were calculated using GraFitVs. 5.013, Erithacus Software Ltd.

Covalent docking calculations. AD4[35-36] was employed for the docking calculations. In this case, as the ligands covalently bind to the enzyme, it was necessary to employ a specific docking protocol devised by Bianco et al.,[37] namely the "flexible side chain method". The latter requires to modify the residue which takes part in the covalent bond and to attach it to the ligand; during the docking calculation, this modified residue is treated as flexible. To this end, using the Maestro suite,[56] we modeled ligands **4a-o** with two extra atoms where the alkylation would take place. Specifically a sulfur and a carbon atom, in order to match the corresponding atoms in the C25. The crystal structure of rhodesain from the Protein Data Bank (PDB code 2P86)[18] was downloaded and prepared for docking using the Protein Preparation Wizard tool in Maestro. Then, with the help of the scripts provided by the AD4 website,[57] it was possible to overlap the ligand with the C25 residue. Then, the receptor grid was calculated with the AutoGrid4 software, mapping the interaction energies of the receptor using the ligand atom types as probes. The grid of 60 Å × 60 Å × 60 Å with 0.375 Å spacing was centered on the coordinates of the ligand originally present in the 2P86 crystal. Finally, the actual docking was run for each compound separately, keeping the remodeled residue as flexible. This allowed sampling the torsional degrees of freedom of the ligands in order to optimize the interactions of the bound ligand with the surrounding residues. For the simulations, the Lamarckian Genetic Algorithm (LGA) was employed. Given the complexity of the ligands and their high number of torsional degrees of freedom, 200 runs of LGA were executed for each compound. Each docking run consisted of 20 million energy evaluations using the Lamarckian genetic algorithm local search (GALS) method. The GALS method evaluates a population of possible docking solutions and

propagates the most successful individuals from each generation into the subsequent generation of possible solutions. A low-frequency local search according to the method of Solis and Wets is applied to docking trials to ensure that the final solution represents a local minimum. All dockings described in this paper were performed with a population size of 150, and 300 rounds of Solis and Wets local search were applied with a probability of 0.06. A mutation rate of 0.02 and a crossover rate of 0.8 were used to generate new docking trials for subsequent generations, and the best individual from each generation was propagated over the next generation. All the other settings were left at their default value. The docking results from each calculation were clustered on the basis of root-mean square deviation (rmsd) (solutions differing by less than 2.0 Å) between the Cartesian coordinates of the atoms and were ranked on the basis of free energy of binding (ΔG_{AD4}). All the images were rendered using the UCSF Chimera Molecular Modeling Software.[58]

Physicochemical and pharmacokinetic properties calculation. These values were *in silico* calculated through the QikProp tool, part of the Schrödinger suite (Schrödinger Release 2019-1: QikProp, Schrödinger, LLC, New York, NY, 2019), using default values.

ASSOCIATED CONTENT

Supporting Information.

The following files are available free of charge:

Table S1

Complex_3 (PDB)

Complex_4h (PDB)

Molecular formula strings (CSV)

AUTHOR INFORMATION

Corresponding Author

* E-mail: rettari@unime.it. Phone: + 39-090-6766554.

ORCID

Roberta Ettari: 0000-0001-9020-2068

Notes

The authors declare no competing financial interest.

ACKNOWLEDGEMENTS

This work was financially supported by the "Fondo per il finanziamento delle attività base di ricerca" (FFABR 2017) financed by MIUR. S.M. acknowledges the support of "Programma Operativo Fondo Sociale Europeo (FSE) Regione Siciliana 2014–2020 – Asse 3 Ob. 10.5″ for her PhD fellowship.

ABBREVIATIONS USED

HAT, Human African Trypanosomiasis; BS, bloodstream; VSG, variant surface glycoprotein; BBB, blood brain barrier; PDB, Protein Data Bank; hPhe: homophenylalanine; HOBt, Hydroxybenzotriazole; EDCI, 1-Ethyl-3-(3-dimethylaminopropyl)carbodiimide; CM, cross-metathesis; THF, tetrahydrofuran; DMF, dimethylformamide; DIPEA, *N*,*N*-Diisopropylethylamine; MW, micro-wave; TLC, thin layer chromatography; Cbz, carbobenzyloxy; AMC, 7-Amino-4-methylcoumarin; DMSO, dimethylsulfoxide; EtOAc, ethyl acetate; EDTA, Ethylenediamine tetraacetic acid; DTT, dithiothreitol.

REFERENCES

(1) Human African Trypanosomiasis; World Health Organization: Geneva, 2018; https://www.who.int/trypanosomiasis_african/en/ (March 20, 2019).

(2) Büscher, P.; Cecchi, G.; Jamonneau, V.; Priotto, G. Human African Trypanosomiasis. *Lancet* **2017**, *390*, 2397-2409.

(3) MacLean, L.; Reiber, H.; Kennedy, P. G.; Sternberg, J. M. Stage Progression and Neurological Symptoms in Trypanosoma Brucei Rhodesiense Sleeping Sickness: Role of the CNS Inflammatory Response. *PLoS Negl. Trop. Dis.* **2012**, *6*, e1857.

(4) Mugnier, M. R.; Cross, G. A.; Papavasiliou, F. N. The in Vivo Dynamics of Antigenic Variation in Trypanosoma Brucei. *Science* **2015**, *347*, 1470-1473.

(5) Babokhov, P.; Sanyaolu, A. O.; Oyibo, W. A.; Fagbenro-Beyioku, A. F.; Iriemenam, N. C. A Current Analysis of Chemotherapy Strategies for the Treatment of Human African Trypanosomiasis. *Pathog. Glob. Health.* **2013**, *107*, 242-252.

(6) Priotto, G.; Kasparian, S.; Mutombo, W.; Ngouama, D.; Ghorashian, S.; Arnold, U.; Ghabri, S.; Baudin, E.; Buard, V.; Kazadi-Kyanza, S.; Ilunga, M.; Mutangala, W.; Pohlig, G.; Schmid, C.; Karunakara, U.; Torreele, E.; Kande, V. Nifurtimox-Eflornithine Combination Therapy for Second-Stage African Trypanosoma Brucei Gambiense Trypanosomiasis: A Multicentre, Randomised, Phase III, Non-Inferiority Trial. *Lancet* **2009**, *374*, 56-64.

(7) Kansiime, F.; Adibaku, S.; Wamboga, C.; Idi, F.; Kato, C. D.; Yamuah, L.; Vaillant, M.; Kioy, D.; Olliaro, P.; Matovu, E. A Multicentre, Randomised, Non-Inferiority Clinical Trial Comparing a Nifurtimox-Eflornithine Combination to Standard Eflornithine Monotherapy for Late Stage Trypanosoma Brucei Gambiense Human African Trypanosomiasis in Uganda. *Parasit. Vectors* **2018**, *11*, 105-115.

(8) EMA/791484/2018 Committee for Medicinal Products for Human Use (CHMP). November 15, 2018.

(9) Ettari, R.; Previti, S.; Tamborini, L.; Cullia, G.; Grasso, S.; Zappalà, M. The Inhibition of Cysteine Proteases Rhodesain and TbCatB: A Valuable Approach to Treat Human African Trypanosomiasis. *Mini Rev. Med. Chem.* **2016**, *16*, 1374-1391.

(10) Ettari, R.; Tamborini, L.; Angelo, I. C.; Micale, N.; Pinto, A.; De Micheli, C.; Conti, P. Inhibition of Rhodesain as a Novel Therapeutic Modality for Human African Trypanosomiasis. *J. Med. Chem.* **2013**, *56*, 5637-5658.

(11) Steverding, D.; Sexton, D. W.; Wang, X.; Gehrke, S. S.; Wagner, G. K.; Caffrey, C. R. Trypanosoma Brucei: Chemical Evidence That Cathepsin L Is Essential for Survival and a Relevant Drug Target. *Int. J. Parasitol.* **2012**, *42*, 481-488.

(12) Nikolskaia, O. V.; de, A. L. A. P.; Kim, Y. V.; Lonsdale-Eccles, J. D.; Fukuma, T.; Scharfstein, J.; Grab, D. J. Blood-Brain Barrier Traversal by African Trypanosomes Requires Calcium Signaling Induced by Parasite Cysteine Protease. *J. Clin. Invest.* **2006**, *116*, 2739-2747.

(13) Triggs, V. P.; Bangs, J. D. Glycosylphosphatidylinositol-Dependent Protein Trafficking in Bloodstream Stage Trypanosoma Brucei. *Eukaryot. Cell* **2003**, *2*, 76-83.

(14) Santos, C. C.; Coombs, G. H.; Lima, A. P.; Mottram, J. C. Role of the Trypanosoma Brucei Natural Cysteine Peptidase Inhibitor ICP in Differentiation and Virulence. *Mol. Microbiol.* **2007**, *66*, 991-1002.

(15) Lalmanach, G.; Boulange, A.; Serveau, C.; Lecaille, F.; Scharfstein, J.; Gauthier, F.; Authie, E. Congopain from Trypanosoma Congolense: Drug Target and Vaccine Candidate. *Biol. Chem.* **2002**, *383*, 739-749.

(16) Caffrey, C. R.; Hansell, E.; Lucas, K. D.; Brinen, L. S.; Alvarez Hernandez, A.; Cheng, J.; Gwaltney, S. L., 2nd; Roush, W. R.; Stierhof, Y. D.; Bogyo, M.; Steverding, D.; McKerrow, J. H. Active Site Mapping, Biochemical Properties and Subcellular Localization of Rhodesain, the Major Cysteine Protease of Trypanosoma Brucei Rhodesiense. *Mol. Biochem. Parasitol.* **2001**, *118*, 61-73.

(17) Kerr, I. D.; Lee, J. H.; Farady, C. J.; Marion, R.; Rickert, M.; Sajid, M.; Pandey, K. C.; Caffrey, C. R.; Legac, J.; Hansell, E.; McKerrow, J. H.; Craik, C. S.; Rosenthal, P. J.; Brinen, L. S. Vinyl Sulfones as Antiparasitic Agents and a Structural Basis for Drug Design. *J. Biol. Chem.* **2009**, *284*, 25697-25703.

(18) Kerr, I. D.; Wu, P.; Marion-Tsukamaki, R.; Mackey, Z. B.; Brinen, L. S. Crystal Structures of TbCatB and Rhodesain, Potential Chemotherapeutic Targets and Major Cysteine Proteases of Trypanosoma Brucei. *PLoS Negl. Trop. Dis.* **2010**, *4*, e701.

(19) Ettari, R.; Previti, S.; Cosconati, S.; Maiorana, S.; Schirmeister, T.; Grasso, S.; Zappalà, M. Development of Novel 1,4-Benzodiazepine-Based Michael Acceptors as Antitrypanosomal Agents. *Bioorg. Med. Chem. Lett.* **2016**, *26*, 3453-3456.

(20) Ettari, R.; Previti, S.; Cosconati, S.; Kesselring, J.; Schirmeister, T.; Grasso, S.; Zappalà, M. Synthesis and Biological Evaluation of Novel Peptidomimetics as Rhodesain Inhibitors. *J. Enzyme Inhib. Med. Chem.* **2016**, *31*, 1184-1191.

(21) Ettari, R.; Pinto, A.; Previti, S.; Tamborini, L.; Angelo, I. C.; La Pietra, V.; Marinelli, L.; Novellino, E.; Schirmeister, T.; Zappalà, M.; Grasso, S.; De Micheli, C.; Conti, P. Development of Novel Dipeptide-Like Rhodesain Inhibitors Containing the 3-Bromoisoxazoline Warhead in a Constrained Conformation. *Bioorg. Med. Chem.* **2015**, *23*, 7053-7060.

(22) Ettari, R.; Pinto, A.; Tamborini, L.; Angelo, I. C.; Grasso, S.; Zappalà, M.; Capodicasa, N.; Yzeiraj, L.; Gruber, E.; Aminake, M. N.; Pradel, G.; Schirmeister, T.; De Micheli, C.; Conti, P. Synthesis and Biological Evaluation of Papain-Family Cathepsin L-Like Cysteine Protease Inhibitors Containing a 1,4-Benzodiazepine Scaffold as Antiprotozoal Agents. *ChemMedChem* **2014**, *9*, 1817-1825.

(23) Rotondo, A.; Ettari, R.; Zappalà, M.; De Micheli, C.; Rotondo, E. Nmr Characterization and Conformational Analysis of a Potent Papain-Family Cathepsin L-Like Cysteine Protease Inhibitor with Different Behaviour in Polar and Apolar Media. *J. Mol. Struct.* **2014**, *1076*, 337-343.

(24) Ettari, R.; Tamborini, L.; Angelo, I. C.; Grasso, S.; Schirmeister, T.; Lo Presti, L.; De Micheli, C.; Pinto, A.; Conti, P. Development of Rhodesain Inhibitors with a 3-Bromoisoxazoline Warhead. *ChemMedChem* **2013**, *8*, 2070-2076.

(25) Ettari, R.; Zappalà, M.; Micale, N.; Schirmeister, T.; Gelhaus, C.; Leippe, M.; Evers, A.; Grasso, S. Synthesis of Novel Peptidomimetics as Inhibitors of Protozoan Cysteine Proteases Falcipain-2 and Rhodesain. *Eur. J. Med. Chem.* **2010**, *45*, 3228-3233.

(26) Previti, S.; Ettari, R.; Cosconati, S.; Amendola, G.; Chouchene, K.; Wagner, A.; Hellmich, U. A.; Ulrich, K.; Krauth-Siegel, R. L.; Wich, P. R.; Schmid, I.; Schirmeister, T.; Gut, J.; Rosenthal, P.

J.; Grasso, S.; Zappalà, M. Development of Novel Peptide-Based Michael Acceptors Targeting Rhodesain and Falcipain-2 for the Treatment of Neglected Tropical Diseases (NTDs). *J. Med. Chem.* **2017**, *60*, 6911-6923.

(27) Yang, P. Y.; Wang, M.; Li, L.; Wu, H.; He, C. Y.; Yao, S. Q. Design, Synthesis and Biological Evaluation of Potent Azadipeptide Nitrile Inhibitors and Activity-Based Probes as Promising Anti-Trypanosoma Brucei Agents. *Chem. Eur. J.* **2012**, *18*, 6528-6541.

(28) Jaishankar, P.; Hansell, E.; Zhao, D. M.; Doyle, P. S.; McKerrow, J. H.; Renslo, A. R. Potency and Selectivity of P2/P3-Modified Inhibitors of Cysteine Proteases from Trypanosomes. *Bioorg. Med. Chem. Lett.* **2008**, *18*, 624-628.

(29) Mott, B. T.; Ferreira, R. S.; Simeonov, A.; Jadhav, A.; Ang, K. K.; Leister, W.; Shen, M.; Silveira, J. T.; Doyle, P. S.; Arkin, M. R.; McKerrow, J. H.; Inglese, J.; Austin, C. P.; Thomas, C. J.; Shoichet, B. K.; Maloney, D. J. Identification and Optimization of Inhibitors of Trypanosomal Cysteine Proteases: Cruzain, Rhodesain, and TbCatB. *J. Med. Chem.* **2010**, *53*, 52-60.

(30) Ettari, R.; Nizi, E.; Di Francesco, M. E.; Dude, M. A.; Pradel, G.; Vicik, R.; Schirmeister, T.; Micale, N.; Grasso, S.; Zappalà, M. Development of Peptidomimetics with a Vinyl Sulfone Warhead as Irreversible Falcipain-2 Inhibitors. *J. Med. Chem.* **2008**, *51*, 988-996.

(31) Ettari, R.; Micale, N. Chloro-Substituted Hoveyda-Grubbs Ruthenium Carbene: Investigation of Electronic Effetcs. *J. Organomet. Chem.* **2007**, *692*, 3574-3576.

(32) Schirmeister, T.; Kesselring, J.; Jung, S.; Schneider, T. H.; Weickert, A.; Becker, J.; Lee, W.; Bamberger, D.; Wich, P. R.; Distler, U.; Tenzer, S.; Johé, P.; Hellmich, U. A.; Engels, B. Quantum Chemical-Based Protocol for the Rational Design of Covalent Inhibitors. *J. Am. Chem. Soc.* **2016**, *138*, 8332-8335.

(33) Pandey, K. C.; Wang, S. X.; Sijwali, P. S.; Lau, A. L.; McKerrow, J. H.; Rosenthal, P. J. The Plasmodium Falciparum Cysteine Protease Falcipain-2 Captures Its Substrate, Hemoglobin, Via a Unique Motif. *Proc. Natl. Acad. Sc.i U.S.A.* **2005**, *102*, 9138-9143.

(34) Powers, J. C.; Asgian, J. L.; Ekici, O. D.; James, K. E. Irreversible Inhibitors of Serine, Cysteine, and Threonine Proteases. *Chem. Rev.* **2002**, *102*, 4639-4750.

(35) Cosconati, S.; Forli, S.; Perryman, A. L.; Harris, R.; Goodsell, D. S.; Olson, A. J. Virtual Screening with Autodock: Theory and Practice. *Expert Opin. Drug Discovery* **2010**, *5*, 597-607.

(36) Morris, G. M.; Huey, R.; Lindstrom, W.; Sanner, M. F.; Belew, R. K.; Goodsell, D. S.; Olson, A. J. AutoDock4 and AutoDockTools4: Automated Docking with Selective Receptor Flexibility. *J. Comput. Chem.* **2009**, *30*, 2785-2791.

(37) Bianco, G.; Forli, S.; Goodsell, D. S.; Olson, A. J. Covalent Docking Using Autodock: Two-Point Attractor and Flexible Side Chain Methods. *Protein Sci.* **2016**, *25*, 295-301.

(38) Ahn, D. S.; Park, S. W.; Lee, S.; Kim, B. Effects of Substituting Sroup on the Hydrogen Bonding in Phenol−H_2O Complexes: Ab Initio Study. *J. Phys. Chem. A* **2003**, *107*, 131-139.

(39) Fu, Z.; He, J.; Tong, A.; Xie, Y.; Wei, Y. A Convenient and Efficient Synthesis of Dipeptidyl Benzoxaboroles and Their Peptidomimetics. *Synthesis* **2013**, *45*, 2843-2852.

(40) Spyropoulos, C.; Kokotos, C. G. One-Pot Synthesis of Ureas from Boc-Protected Amines. *J. Org. Chem.* **2014**, *79*, 4477-4483.

(41) Tomita, K.; Oishi, S.; Ohno, H.; Fujii, N. Structure-Activity Relationship Study and NMR Analysis of Fluorobenzoyl Pentapeptide GPR54 Agonists. *Biopolymers* **2008**, *90*, 503-511.

(42) Tu, G. G.; Yan, Y. G.; Chen, X. Y.; Lv, Q. L.; Wang, J. Q.; Li, S. H. Synthesis and Antiproliferative Assay of 1,3,4-Oxadiazole and 1,2,4-Triazole Derivatives in Cancer Cells. *Drug Discov. Ther.* **2013**, *7*, 58-65.

(43) Fennell, B. D.; Warren, J. M.; Chung, K. K.; Main, H. L.; Arend, A. B.; Tochowicz, A.; Gotz, M. G. Optimization of Peptidyl Allyl Sulfones as Clan CA Cysteine Protease Inhibitors. *J. Enzyme Inhib. Med. Chem.* **2013**, *28*, 468-478.

(44) Benvenuti, S.; Severi, F.; Costantino, L.; Vampa, G.; Melegari, M. Synthesis and Aldose Reductase Inhibitory Activity of Benzoyl-Amino Acid Derivatives. *Il Farmaco* **1998**, *53*, 439-442.

(45) Pejchalová, M.; Havelek, R.; Královec, K.; Růžičková, Z.; Pejchal, V. Novel Derivatives of Substituted 6-Fluorobenzothiazole Diamides: Synthesis, Antifungal Activity and Cytotoxicity. *Med. Chem. Res.* **2017**, *26*, 1847-1862.

(46) Skogh, A.; Friis, S. D.; Skrydstrup, T.; Sandstrom, A. Palladium-Catalyzed Aminocarbonylation in Solid-Phase Peptide Synthesis: A Method for Capping, Cyclization, and Isotope Labeling. *Org. Lett.* **2017**, *19*, 2873-2876.

(47) Draper, R. W.; Hou, D.; Iyer, R.; Lee, G. M.; Liang, J. T.; Mas, J. L.; Vater, E. J. Novel Stereoselective Syntheses of the Fused Benzazepine Dopamine D-1 Antagonist (6aS,13bR)-11-Chloro-6,6a,7,8,9,13b-hexahydro-7-methyl-5H-Benzo[d]naphth[2,1-b]azepin-12-ol (Sch 39166): 2. L-Homophenylalanine-Based Syntheses. *Org. Proc. Res. Dev.* **1998**, *2*, 186-193.

(48) Wagner, A.; Le, T. A.; Brennich, M.; Klein, P.; Bader, N.; Diehl, E.; Paszek, D.; Weickhmann, A. K.; Dirdjaja, N.; Krauth-Siegel, R. L.; Engels, B.; Opatz, T.; Schindelin, H.; Hellmich, U. A. Inhibitor-Induced Dimerization of an Essential Oxidoreductase from African Trypanosomes. *Angew. Chem. Int. Ed. Engl.* **2019**, *58*, 3640-3644.

(49) Latorre, A.; Schirmeister, T.; Kesselring, J.; Jung, S.; Johé, P.; Hellmich, U. A.; Heilos, A.; Engels, B.; Krauth-Siegel, R. L.; Dirdjaja, N.; Bou-Iserte, L.; Rodríguez, S.; González, F. V. Dipeptidyl Nitroalkenes as Potent Reversible Inhibitors of Cysteine Proteases Rhodesain and Cruzain. *ACS Med. Chem. Lett.* **2016**, *7*, 1073-1076.

(50) Tian, W. X.; Tsou, C. L. Determination of the Rate Constant of Enzyme Modification by Measuring the Substrate Reaction in the Presence of the Modifier. *Biochemistry* **1982**, *21*, 1028-1032.

(51) GraFit, Version 5.0.1.3; Erithacus Software Ltd.: London, 2006.

(52) Vicik, R.; Hoerr, V.; Glaser, M.; Schultheis, M.; Hansell, E.; McKerrow, J. H.; Holzgrabe, U.; Caffrey, C. R.; Ponte-Sucre, A.; Moll, H.; Stich, A.; Schirmeister, T. Aziridine-2,3-Dicarboxylate Inhibitors Targeting the Major Cysteine Protease of Trypanosoma Brucei as Lead Trypanocidal Agents. *Bioorg. Med. Chem. Lett.* **2006**, *16*, 2753-2757.

(53) Cunningham, M. P.; Vickerman, K. Antigenic Analysis in the Trypanosoma Brucei Group, Using the Agglutination Reaction. *Trans. R. Soc. Trop. Med. Hyg.* **1962**, *56*, 48-59.

(54) Hirumi, H.; Hirumi, K. Continuous Cultivation of Trypanosoma brucei Blood Stream Forms in a Medium Containing a Low Concentration of Serum Protein without Feeder Cell Layers. *The Journal of Parasitology* **1989**, *75*, 985-989.

(55) Crouch, S. P.; Kozlowski, R.; Slater, K. J.; Fletcher, J. The Use of ATP Bioluminescence as a Measure of Cell Proliferation and Cytotoxicity. *J. Immunol. Methods* **1993**, *160*, 81-88.

(56) Schrödinger Maestro Release 2018-3, Schrödinger, LLC, New York, NY, 2018.

(57) AutoDock; Molecular Graphics Laboratory: La Jolla, CA, 2013; http://autodock.scripps.edu/ (January 13, 2016).

(58) UCSF Chimera: An Extensible Molecular Modeling System; University of California, San Francisco: San Francisco, 2017; http://www.rbvi.ucsf.edu/chimera/ (September 13, 2016).

Table of content graphics.

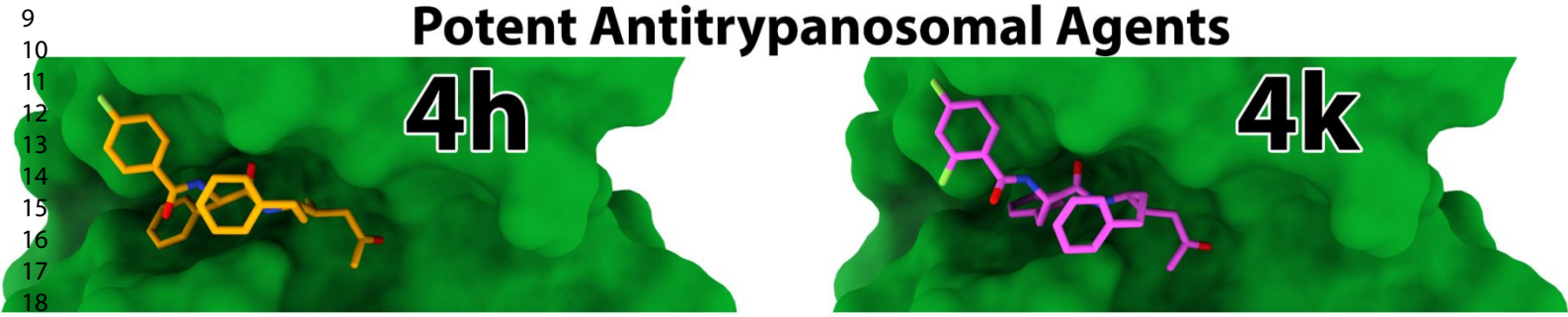

Rhodesain k_{2nd} 88.1 · 10^7 M^{-1} min^{-1}; K_i 0.0011 nM
T. brucei brucei EC_{50} 3.6 µM

Rhodesain k_{2nd} 107.1 · 10^7 M^{-1} min^{-1}; K_i 0.0006 nM
T. brucei brucei EC_{50} 0.67 µM